

Neutrino Oscillations as a Gravitational Wave Detector?

Dominik Hellmann^{1*}, Sara Krieg^{1†}, Heinrich Päs^{1‡}, Mustafa Tabet^{1§}

¹ *Fakultät für Physik, Technische Universität Dortmund, Germany*

May 9, 2024

Abstract

Gravitational Waves (GWs) can alter the neutrino propagation distance and thus affect neutrino oscillations. This can result in a complete disappearance of the oscillatory behavior that competes with other sources of neutrino decoherence. We develop a set of criteria that determines under which conditions neutrino oscillations are sensitive to this effect, and discuss three concrete scenarios for neutrinos from astrophysical sources. We find that neutrino oscillations may probe so far unexplored regions of the GW parameter space.

1 Introduction

Gravitational wave (GW) astronomy provides a new window for our exploration of the universe. This includes the observation of previously inaccessible phenomena, such as the merger of black holes [1] and allows for the investigation and detection of neutron star mergers [2], collisions between neutron stars and black holes [3], and potentially the explosion of supernovae in the future [4]. Moreover, GWs can be employed in the search for exotic objects such as cosmic strings [5] or primordial black holes [6], and thus provide clues to physics beyond the Standard Model (SM). In principle GWs in the sub nHz range may even provide novel possibilities to constrain inflationary models [7]. Recent achievements like NANOGrav's detection of evidence for a GW background using pulsar timing arrays (PTAs) [8] prove that we are at the beginning of an exciting new era of GW and multimessenger astronomy. Further efforts are underway to expand the capabilities of existing gravitational wave detectors such as LIGO and Virgo, while plans for next generation detectors like the Einstein Telescope [9] and LISA (Laser Interferometer Space Antenna) [10] promise an even greater sensitivity and a broader range of observations in the near future.

While much attention has been focused on the detection and characterization of GWs using conventional methods, such as laser interferometry [11], there is a growing recognition of the potential role that neutrinos could play in this area of research [12–21]. As has been already pointed out in references [22–29], gravitational fields modify the time evolution phase of quantum particles. Since neutrinos are able to traverse vast distances through astrophysical environments without being deflected from their trajectory, they could offer unique insights into the GW landscape. One promising research direction is to study how GWs affect quantum interference phenomena like neutrino flavor oscillations.

So far, most works on this subject consider the influence of a stochastic GW background (SGWB) as a source of quantum decoherence in neutrino oscillations, see for example references [12–19]. In this work we argue that not only stochastic perturbations of the neutrino evolution phase can cause decoherence in the neutrino system, but that also GW signals from individual sources will at least in principle have a similar effect that may be searched for. We discuss in detail the challenges and prospects of such an approach and investigate the importance of the interplay of GW induced decoherence with other sources of decoherence, as described by references [30–40]. These decoherence effects arise, for example, from the separation of neutrino wave packets,

*dominik.hellmann@tu-dortmund.de

†sara.krieg@tu-dortmund.de

‡heinrich.paes@tu-dortmund.de

§mustafa.tabet@tu-dortmund.de

potentially macroscopic neutrino production regions and finite energy binning and result in a similar damping of the oscillation behavior of neutrino flavor transitions. Therefore it is important to account for these effects in a coherent statistical treatment in order to determine if an experiment would, in principle, be sensitive to the GW induced effect, a step that has not yet been undertaken in previous studies.

This paper is organized as follows. In section 2 we develop a simple yet robust heuristic model accounting for the effects of the curved spacetime induced by GWs on neutrino propagation by considering deviations from the static trajectory approximation. A time average of the oscillation probability over the running time of a neutrino experiment is employed in order to account for a varying travel distance and to predict the expected neutrino oscillation pattern. In section 3 we develop several criteria that determine whether neutrino oscillations can be sensitive to GWs, and constrain the amplitudes and frequencies of GWs that can be probed within this framework. In section 4 we study concrete scenarios for the impact of GWs on neutrino oscillations, starting with baselines smaller than the diameter of the solar system in section 4.1. Baselines exceeding the diameter of the solar system using the example of the Vela pulsar are considered in section 4.2, and in section 4.3 we investigate neutrino oscillations in presence of a SGWB. A summary and conclusions are provided in section 5. Technical details regarding the calculation and the statistical method employed for the analyses can be found in the appendices, where we also comment on further potential scenarios.

2 Modified Oscillation Probability in the Presence of Gravitational Waves

To investigate how the propagation of neutrinos through a curved spacetime induced by GWs affects their flavor oscillations, we start with the standard neutrino oscillation probability

$$\hat{P}_{ab}(E, L) = \sum_j |U_{aj}|^2 |U_{bj}|^2 + 2 \sum_{j < k} \text{Re} \left(U_{aj}^* U_{bj} U_{ak} U_{bk}^* \exp \left[-2\pi i \frac{L}{L_{jk}^{\text{osc}}} - \mathcal{D}_{jk}(E, L) \right] \right), \quad (1)$$

where \mathcal{D}_{jk} is a positive damping term describing the decoherence due to wave packet separation and $L_{jk}^{\text{osc}} = 4\pi E / \Delta m_{jk}^2$ is the oscillation length. The matrix U describes the neutrino mixing, e.g. for three neutrino flavors U corresponds to the Pontecorvo–Maki–Nakagawa–Sakata (PMNS) matrix, $\Delta m_{jk}^2 = m_j^2 - m_k^2$ are the squared mass splittings of the neutrino mass eigenstates and E is the average energy of the neutrino system. Depending on the shape of the neutrino wave packets the decoherence function \mathcal{D}_{jk} can differ. A common assumption for the neutrino wave packets is that they are of Gaussian shape implying

$$\mathcal{D}_{jk}(E, L) = \left(\frac{L}{L_{jk}^{\text{coh}}} \right)^2 \quad \text{with} \quad L_{jk}^{\text{coh}} = 2\sqrt{2} \frac{\sigma_x}{|\Delta v_{jk}|} \quad \text{and} \quad \Delta v_{jk} = \frac{\Delta m_{jk}^2}{2E^2}, \quad (2)$$

with the position space wave packet width σ_x that we take to be equal for all mass eigenstates for simplicity.

We now describe how GWs influence neutrino oscillations by modifying the length L in the standard probability, cf. equation (1), and replacing it with the propagation distance of neutrinos in curved spacetime. For this, we consider the average geodesic γ that the neutrino wave packets follow which now are slightly perturbed due to the presence of the GW,

$$\gamma_0^\mu(\tau) = \underbrace{\frac{X_D^\mu - X_P^\mu}{\tau_D - \tau_P}}_{w^\mu} (\tau - \tau_P) + X_P^\mu \quad \longrightarrow \quad \gamma^\mu(\tau) = \gamma_0^\mu(\tau) + \Delta\gamma^\mu(\tau), \quad (3)$$

where $X_{P(D)}^\mu$ denote the coordinates of neutrino production (detection), τ is the proper time parameterizing the neutrino geodesic and hence $\tau_{P(D)}$ denote its corresponding value at production (detection), respectively. To obtain the first order correction $\Delta\gamma$ to the flat spacetime geodesic γ_0 , we solve the geodesic equation for the metric¹ $g_{\mu\nu} = \eta_{\mu\nu} + h_{\mu\nu}$ with the perturbation to flat space time $h_{\mu\nu}$, describing the GW, with boundary values² X_P^μ and X_D^μ . For the step by step calculation see appendix A.

¹In this work we use the west coast convention, i.e. $\eta = \text{diag}(+1, -1, -1, -1)$.

²Especially we assume that this problem is well posed, i.e. that geodesics connecting those points are unique.

The spatial length L that neutrino wave packets have traveled between production and detection coordinate time t_P and t_D is given by

$$L(t_P, t_D) = \int_{\tau_P}^{\tau_D} \sqrt{-g_{jk}(\gamma(\tau)) \dot{\gamma}^j(\tau) \dot{\gamma}^k(\tau)} d\tau \quad (4)$$

$$\approx L_0 - \frac{u^0}{2} \int_{\tau_P}^{\tau_D} h_{\parallel}(\gamma_0(t)) d\tau =: L_0 + \Delta L, \quad (5)$$

which is then substituted into the standard oscillation probability. Here h_{\parallel} is the metric perturbation projected onto the zeroth order neutrino trajectory γ_0 . Moreover, we use the ultrarelativistic approximation for the neutrino velocity and neglect terms of $\mathcal{O}(h^2)$ in order to express the detection time as $t_D \approx L_0 + t_P \equiv L_0 + t$. For the details of the calculation see Appendix B. In order to evaluate the proper time intergration in equation (5), we use the fact that any GW can be decomposed into plus and cross polarized plane waves, i.e.

$$h_{\mu\nu}(x) = \sum_{r \in \{+, \times\}} \int d^3\vec{k} \psi_r(\vec{k}) A_{\mu\nu}^r \cos(\omega t - \vec{k}\vec{x} + \phi^r(\vec{k})), \quad (6)$$

where $A_{\mu\nu}^r$ are normalized polarization tensors, $\psi_r(\vec{k})$ are real, positive momentum space wave packets and $\phi^r(\vec{k})$ denote the phase shifts of the corresponding modes. Exploiting this decomposition, equation (5) becomes

$$\Delta L(t) \approx -\frac{1}{2} \sum_{r \in \{+, \times\}} \int d^3\vec{k} \psi_r(\vec{k}) \frac{A_{\parallel}^r(\varphi, \theta)}{\tilde{\omega}} \{ \sin(\tilde{\omega} L_0) \cos(\omega t + \phi^r) + [\cos(\tilde{\omega} L_0) - 1] \sin(\omega t + \phi^r) \}, \quad (7)$$

where θ and φ are the angles defining the relative orientation of the neutrino trajectory γ_0 and the GW propagation direction. In terms of these angles we define the reduced GW frequency, $\tilde{\omega}$, and the projected polarization tensors, $A_{\parallel}^r(\varphi, \theta)$, as

$$\tilde{\omega} := \omega(1 - \cos(\theta)), \quad A_{\parallel}^+(\varphi, \theta) := \sin^2(\theta) \cos(2\varphi), \quad A_{\parallel}^{\times}(\varphi, \theta) := \sin^2(\theta) \sin(2\varphi). \quad (8)$$

Depending on the experimental setup, the angles θ and φ could change with time. This can weaken the overall effect since it is only maximal for constant perpendicular neutrino and GW directions, i.e. $\theta = \pi/2$, see Appendix C for a detailed discussion.

Next, we need to average over the duration of the data taking period T , since neither production nor detection time are usually analyzed in neutrino experiments. Thus, the oscillation probability is given by

$$P_{ab}(E, L_0) = \frac{1}{T} \int_0^T \hat{P}_{ab}(E, L_0 + \Delta L(t)) dt \equiv \langle \hat{P}_{ab}(E, L_0 + \Delta L) \rangle_T. \quad (9)$$

This gives rise to an additional damping of the oscillating terms in the oscillation probability \hat{P} which can be interpreted as a new source of decoherence.

Finally, we need to reconsider the physical meaning of our parameter L_0 . In the comparison of the prediction of the neutrino oscillation pattern with and without the GW effect, L_0 plays the role of the physical distance of neutrino source and detector measured at a certain time t_0 . If a GW of any kind is present in the system this will replace the original value of the parameter L_0 by $\tilde{L}_0 = L_0 + \Delta L(t_0)$. Therefore \tilde{L}_0 is the actual, physical reference length entering the neutrino flavor transition probability implying that equation (9) needs to be evaluated at $L_0 = \tilde{L}_0 - \Delta L(t_0)$, corresponding to the subtraction of a constant off-set. This subtlety is especially important if the GW does not oscillate over a full period during the time of data taking, T , since then the parameter L_0 is unphysical and the actual observable length is \tilde{L}_0 . Hence, only time dependent changes in $L(t)$ can be measured using the method described above. From now on, we eliminate the unphysical parameter L_0 in favor of the physical reference length \tilde{L}_0 from our description and afterwards rename \tilde{L}_0 to L_0 .

In order to gain a better understanding of the impact of GWs on the neutrino oscillation probability, we plot the $\nu_{\mu} \rightarrow \nu_{\mu}$ survival probability in figure 1. For illustration purposes, we choose a baseline of $L_0 = 10^{10}$ km, neutrino energies on the order of $\mathcal{O}(10\text{--}100 \text{ MeV})$, standard neutrino mass and mixing parameters for normal

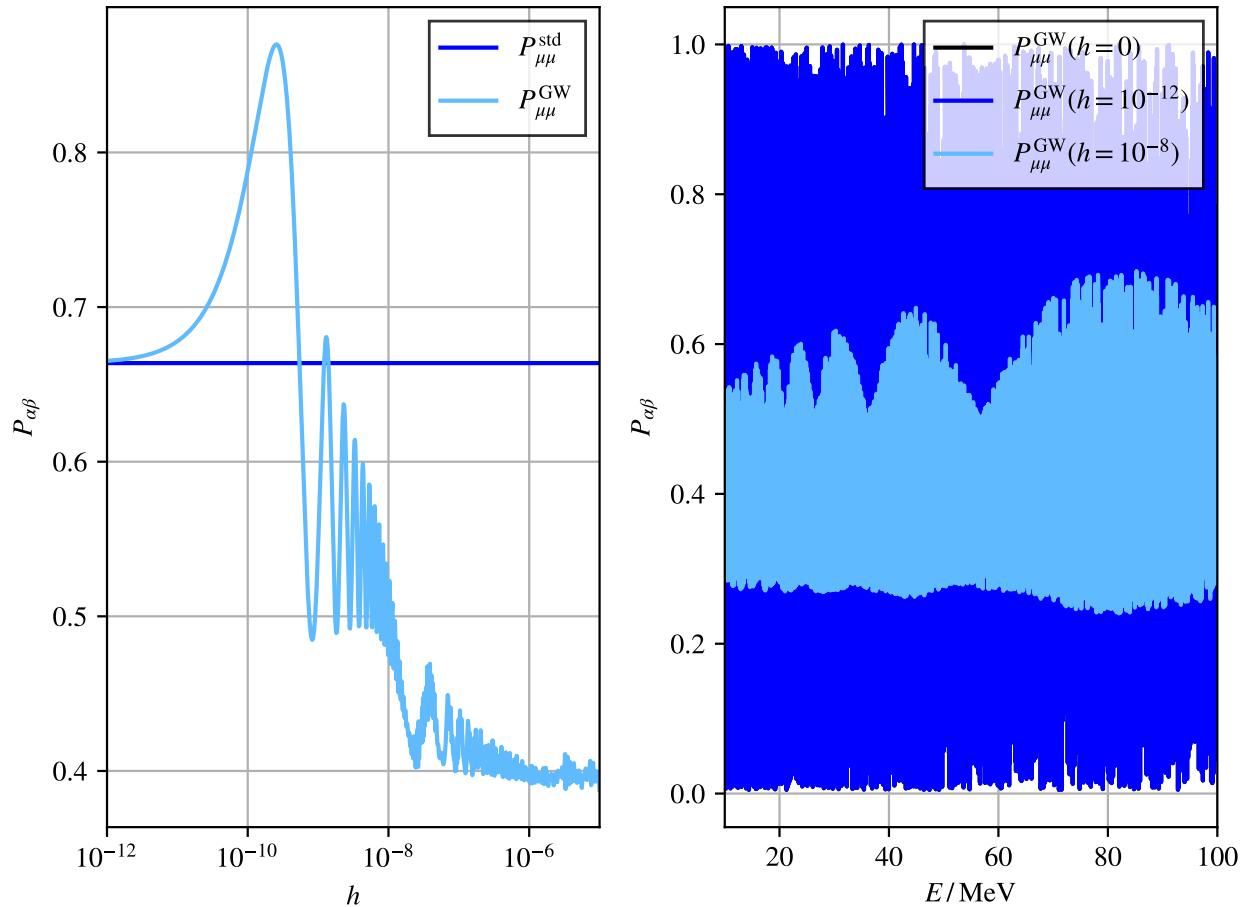


Figure 1: Muon neutrino survival probability, $P_{\mu\mu}$, for different background GWs of different strains h . Left: $P_{\mu\mu}$ with (blue) and without (light blue) the influence of a GW for $E = 10 \text{ MeV}$, $L_0 = 10^{10} \text{ km}$. Right: $P_{\mu\mu}$ for different fixed GW strains $h \in \{0, 10^{-12}, 10^{-8}\}$ and variable energy at $L_0 = 10^{10} \text{ km}$. The black oscillation curve ($h = 0$) almost coincides with the blue curve ($h = 10^{-12}$) and is therefore hidden.

mass ordering [41] and an infinite wave packet width, i.e. we ignore decoherence from wave packet separation. Furthermore, we consider a simple, plus polarized, plane GW with variable strain $\psi_+ \equiv h$ and frequency $f \sim 3 \times 10^{-7} \text{ Hz}$. It is obvious that for small strains, the modified probability coincides with the standard expectation while for larger strains, we expect a significant deviation due to the averaging procedure just described. The non-trivial, oscillating dependence on the strain can be explained by considering the mechanism of averaging the flavor transition probability over time. As the strain increases, so does the amplitude of ΔL and the averaging proceeds over many neutrino oscillation cycles resulting in the stable decoherence limit for large strains. For strains from the intermediate region the time integral only produces averaging over a partial oscillation cycle leading to an average value varying with the strain.

3 General Conditions for Observability of Gravitational Waves Induced Decoherence

In the following, we discuss the conditions that must be fulfilled for the new decoherence effect to be observable in experiments:

- (i) Neutrino oscillations proceed sufficiently rapid such that for given GW parameters the deviation ΔL is comparable to at least one of the oscillation lengths.
- (ii) Decoherence due to wave packet separation occurs later than GW induced decoherence, i.e. at larger baselines or smaller energies.
- (iii) The energy resolution or binning, ΔE , of the neutrino source and detector are sufficiently accurate such that oscillations are not averaged out, i.e. neutrino oscillations have to be sufficiently slow for the experiment to resolve them.
- (iv) The spatial extent of the region of neutrino origin must be much smaller than the oscillation length of the neutrinos to be resolved.
- (v) Neutrino source and detector must not be fixed such that their physical distance can be influenced by the GW.

Unfortunately, requirements one and three compete with each other: On the one hand neutrino oscillations have to be fast enough such that the variation of the deviation ΔL over the run time of the experiment is sufficiently large in order for the time average in equation (9) to damp the oscillations. On the other hand the oscillations must not be too fast since otherwise the finite energy bin width will damp the oscillations, and the effect due to the GW is unresolvable. In the following we further quantify these loosely formulated criteria.

Criterion (i) and (ii) First we examine the maximal deviation ΔL from the baseline L_0 . Since we want to explore the usefulness of neutrino oscillations as probes for coherent GW signals, we now restrict our discussion to plane GWs³. In this case the distance correction ΔL from equation (7) becomes

$$\Delta L(t) \approx -\frac{1}{2\tilde{\omega}} \sum_{r \in \{+, \times\}} a_r A_{\parallel}^r(\varphi, \theta) \{ \sin(\tilde{\omega}L_0) \cos(\omega t + \phi^r) + [\cos(\tilde{\omega}L_0) - 1] \sin(\omega t + \phi^r) \}, \quad (10)$$

with mean frequency ω and polarization amplitudes a_r . It is evident that for a fixed length L_0 the amplitudes appearing in this expression oscillate with respect to the reduced frequency $\tilde{\omega}$. This makes it more difficult to set bounds on the high frequency region $\tilde{\omega} \geq L_0^{-1}$ which is why, for the following discussion, we focus on the low frequency region $\tilde{\omega} \ll L_0^{-1}$. In this region, we can express the maximal baseline deviation as

$$\max_{\omega t \in [0, 2\pi)} |\Delta L(t)| = \frac{hL_0}{2}, \quad (11)$$

with

$$h := \sin^2(\theta) \max_{\omega t \in [0, 2\pi)} |a_+ \cos(2\varphi) \cos(\omega t + \phi^+) + a_{\times} \sin(2\varphi) \cos(\omega t + \phi^{\times})|. \quad (12)$$

For a discernible effect, it is also crucial that the maximum deviation ΔL is comparable to the oscillation length L_{jk}^{osc} of neutrinos:

$$r = \frac{\max_{t \in \tau} |\Delta L(t)|}{L_{jk}^{\text{osc}}} = \frac{\Delta m_{jk}^2}{4\pi E} \frac{hL_0}{2}, \quad (13)$$

where we conservatively choose the ratio $r \approx 0.1$. The reason for this is that the $\nu_j - \nu_k$ interference term needs to be sufficiently damped by the averaging procedure. For each scenario we consider the oscillation term with

³That means GW signals with sufficiently peaked momentum distributions, i.e. $\psi_r(\vec{k}) \approx a_r \delta^{(3)}(\vec{k} - \vec{k}_0)$

the largest mass difference Δm_{jk}^2 , since we are interested in the sensitivity of our framework. However, the decision on which oscillation dominates must be made based on the experiment under consideration. From this we can derive a lower limit on the baseline L_{\min} such that the effect becomes visible, i.e.

$$L_{\min}(E) = 8\pi r \frac{E}{h\Delta m_{jk}^2} < L_0. \quad (14)$$

On the other hand, it is essential for the baseline L to be smaller than the coherence length L_{jk}^{coh} of neutrinos to ensure that the effect of wave packet decoherence does not dominate and thus hide the desired effect. This results in an upper limit implying that the baseline L_0 has to vary within the following window to enable the observation of an effect:

$$L_{\min}(E) < L_0 < L_{jk}^{\text{coh}} \quad (15)$$

$$\Leftrightarrow 8\pi r \frac{E}{h\Delta m_{jk}^2} < L_0 < \frac{4\sqrt{2}E^2}{\Delta m_{jk}^2} \sigma_x. \quad (16)$$

Criterion (iii) and (iv) The energy resolution ΔE must be sufficiently high to resolve the neutrino oscillations by the experiment. This implies that the frequency of the oscillation cannot be too large as too many wave cycles are contained within an energy bin, thus averaging out the effect. In the case of a sinusoidal oscillation of the form $\sin(\omega t)$, this would mean that the period Δt , corresponding to the bin width, should be smaller than the inverse frequency: $\Delta t \lesssim \omega^{-1}$. This consideration can be applied to our case, leading to an energy resolution estimate for the resolution of the jk -oscillation:

$$\left| \Delta \left(\frac{L_0}{E} \right) \right| \lesssim \frac{2}{\Delta m_{jk}^2} \Leftrightarrow \Delta E \lesssim \frac{2}{\Delta m_{jk}^2} \frac{E^2}{L_0}, \quad (17)$$

In addition to energy resolution, position resolution is also relevant. It is important that we know the origin of the neutrinos to a certain degree, hence the width of the production region Σ_P must be smaller than the oscillation length L_{jk}^{osc} to prevent additional averaging hiding the gravitationally induced effect:

$$\Sigma_P \ll L_{jk}^{\text{osc}}. \quad (18)$$

Criterion (v) In the measurement of GW effects, it is crucial to account for the absence of strong forces maintaining a constant physical distance between two reference points. For instance, in the case of LIGO, this is achieved through freely suspended mirrors [42]. In our context, this demands the forces between the detector and the source to be negligible compared to the force of displacement induced by the GW. Astrophysical neutrino sources do not pose a problem in this regard, as detector and source are freely falling in the local gravitational fields. One possibility would be to detect neutrinos from natural sources like the sun or, assuming they exist, decaying dark matter (DM) particles within the gravitational wells of celestial bodies. At even larger distances pulsars, blazars or supernovae are possible candidates for neutrino sources.

Selection of Benchmark Scenarios We can finally use these conditions to find interesting parameter configurations for baselines L_0 , the mass squared difference Δm_{jk}^2 , the neutrino wave packet width σ_x and energy E . For SM neutrinos we know the mass squared differences to be $\Delta m_{21}^2 = 7 \times 10^{-5} \text{ eV}^2$ [41] and $\Delta m_{32}^2 = 2.437 \times 10^{-3} \text{ eV}^2$ [41], respectively, while typical wave packet widths are in the nm range or below [43]. From the condition $\tilde{\omega} > L_0^{-1}$, cf. criterion (i), we can now infer interesting baseline configurations depending on which GW frequencies we want to be sensitive to.

We are particularly interested in frequency ranges of GWs that are not yet explored by other existing or planned experiments. EPTA, IPTA and NANOgrav can cover frequency ranges from roughly 10^{-8} Hz to 10^{-6} Hz [44, 45] and LIGO is sensitive in the range of 10 Hz to 10^4 Hz [46]. The planned experiment LISA and proposed eLISA would be sensitive to frequencies from 10^{-5} Hz to 1 Hz [10]. From this, three frequency ranges

with $f = \omega/(2\pi)$ can be identified that are not yet covered by currently running or approved experiments:

$$f_{\text{GW},1} \lesssim 10^{-9} \text{ Hz}, \quad (19)$$

$$10^{-6} \text{ Hz} \lesssim f_{\text{GW},2} \lesssim 10^{-5} \text{ Hz}, \quad (20)$$

$$1 \text{ Hz} \lesssim f_{\text{GW},3} \lesssim 10 \text{ Hz}. \quad (21)$$

In order to detect an effect, the baseline L_0 should be smaller than f^{-1} . Therefore, we suggest three baselines L_0 :

$$L_{0,1} = 10^5 \text{ km}, \quad (22)$$

$$L_{0,2} = 10^8 \text{ km}, \quad (23)$$

$$L_{0,3} = 10^{10} \text{ km}. \quad (24)$$

All three values are comparable to distances within our solar system, leading us to the experimental challenge discussed above, cf. criterion (v). An additional difficulty arises from the duration of coherent GW signals T_{GW} compared to the data taking period of the neutrino experiment T_{exp} . If $T_{\text{GW}} \ll T_{\text{exp}}$ the averaging effect will be washed out and the sensitivity decreases. Therefore we expect neutrino based GW detection to be most sensitive to astrophysical events emitting GW signals of durations of $\mathcal{O}(10\text{yr})$ or greater, like supermassive blackhole binary (SMBHB) [47] mergers or extreme-mass-ratio inspirals (EMRI) [48]. It is worth noting that SMBHB mergers typically last longer than 10 years while emitting GWs with a constant frequency [49].

Next we want to estimate the sensitivity to the strain of a given GW signal for the parameter configurations discussed above. To this end we show the energy and strain ranges for which we expect an observable effect at the three baselines from equation (22)–(24) of interest in figure 2. Here, the orange line represents the lower limit on the energy E as a function of the strain h for a wave packet width of $\sigma_x = 1 \text{ nm}$ fulfilling the condition in equation (16). The blue line shows the upper limit on the energy E as a function of the strain h for the respective baselines and a mass splitting $\Delta m_{jk}^2 = 10^{-3} \text{ eV}^2$, which results from the condition in equation (14). The intersection of the two lines marks the lowest strain h_{min} that is observable for the scenarios just discussed. To clarify which ranges of strain can realistically be accessed, h_{min} and the corresponding energy E are shown as a function of the baseline L_0 in figure 3. It is evident that the bounds for the strain are several orders of magnitude weaker compared to LIGO and LISA, thus favoring very large length L_0 and energy E combinations. As a consequence, this method is particularly sensitive to SMBHB and EMRI below the frequency range probed by LISA. In the following, we will study more closely how criteria (i)–(v) can be met in concrete scenarios for the potentially interesting baselines $L_{0,1}$, $L_{0,2}$ and $L_{0,3}$ identified above and perform a precise statistical analysis demonstrating that our estimations for the minimum strains h_{min} are indeed accurate.

4 Parameter Constraints for Gravitational Waves: A Toy Analysis

In order to estimate the actual sensitivity of neutrino oscillations on the presence of a GW, we perform a toy analysis for each scenario discussed in the preceding section taking into account all deviations from the standard oscillation pattern. To this end, we model several hypothetical experimental set-ups and estimate the strain and frequency regions they would be sensitive to. Each of these hypothetical experiments is assumed to count neutrino event rates in finite, equal width energy bins and the corresponding neutrino signal is expected to originate from a source at some distance L_0 . We discuss two different classes of sources. First, we assume a peaked neutrino energy spectrum, like for example found for neutrinos from fixed target experiments or from decaying particles at rest, approximated by a Gaussian energy spectrum with width σ_E centered at some mean energy \bar{E} . Second, we assume a power law spectrum for neutrinos from astrophysical environments where charged particles are accelerated in jets and interact with each other or the environment to produce neutrinos.

While the power law dependence is a rather accurate model of a natural neutrino flux, the Gaussian flux is more like a crude approximation to flux shapes exhibiting a peak at a certain energy, \bar{E} . We still adopt this approximation for simplicity because the sensitivity to the GW parameters does not strongly depend on the shape of the flux spectrum as long as there are sufficiently high event counts in the chosen energy range

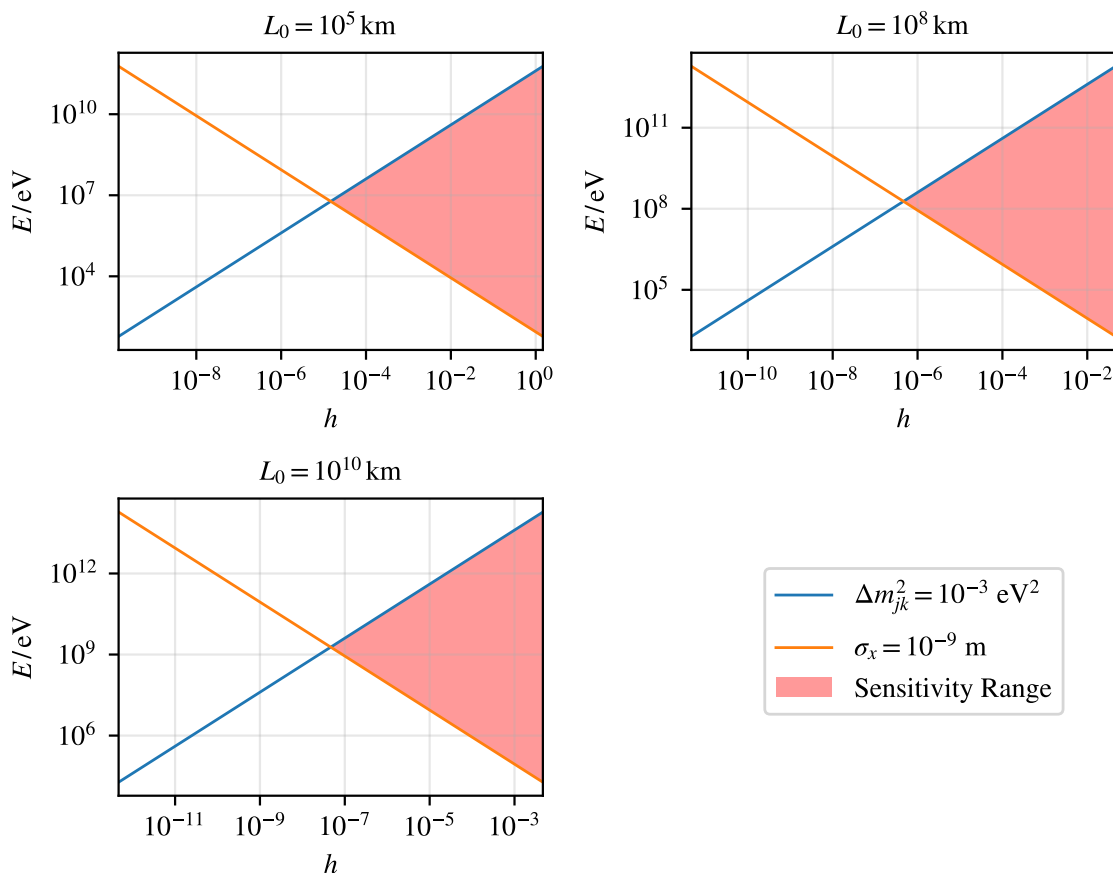


Figure 2: Sensitivity Range determined from the requirement that neutrino oscillations proceed sufficiently rapid (criterion (i)) for fixed baselines L_0 with neutrino mass differences Δm_{jk}^2 consistent with the neutrino oscillation data and neutrino wave packet widths in the nm range. The red area marks the range where neutrino oscillations can be sensitive on GWs in each case, while the blue line marks the upper limit on the energy and the orange line the lower limit as a function of the strain h .

$E \in [E_{\min}, E_{\max}]$. For the same reason we generically choose $\bar{E} = (E_{\max} + E_{\min})/2$ and $\sigma_E = 0.1(E_{\max} - E_{\min})$. The number of neutrino events is then predicted according to the probability density,

$$\rho_b(E) = \sum_a \varphi_a(E) P_{ab}(E, L_0), \quad (25)$$

where φ_a is the neutrino flavor and energy distribution at the source and P_{ab} is the flavor transition probability of the given model.

We generate a toy data set, assuming the expected number of events for each energy and flavor bin to follow the flat spacetime prediction with fixed length L_0 . On this data set, we perform a likelihood ratio test where we evaluate the negative logarithmic likelihood ratio (NLLR) on each point of a region in our parameter space. We only consider “plus” (+) polarized GWs perpendicular to the neutrino trajectory since both possible polarizations are expected to cause a similar effect. Furthermore, we assume a data taking period of $T_{\text{exp}} = 20$ yr for each scenario for the details of the time average, cf. equation(9). For GW frequencies $f \gtrsim T_{\text{exp}}^{-1} \approx 1.6$ nHz the effect of GW induced decoherence is insensitive to the phase ϕ^+ of the GW since we are averaging over multiple cycles of the wave period. Hence, we set it to zero if not stated otherwise.

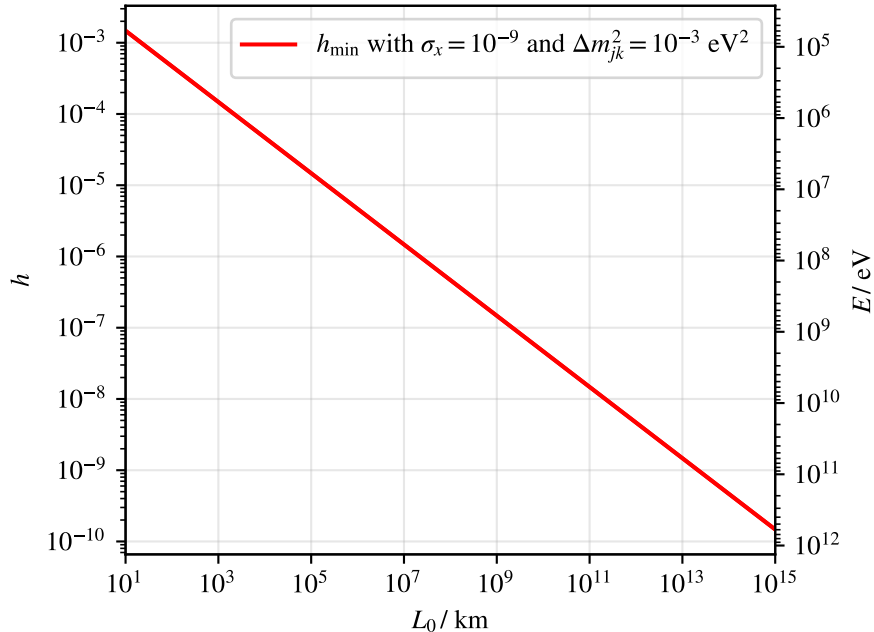


Figure 3: Estimation of the minimally observable strain h_{\min} in the case of SM neutrinos with a neutrino baseline L_0 , energy E and neutrino wave packet width $\sigma_x = 1$ nm.

At frequencies below T_{exp}^{-1} the decoherence effect caused by the GW weakens since ΔL only changes slightly during the data taking period. Thus, we mostly restrict the frequency range to values above this threshold. It is only for neutrinos from galactic pulsars where we also consider lower frequencies and discuss the implications of the slow variation of ΔL .

The remaining parameter space is two dimensional and consists of the possible strain, h , and frequency values, f . Further details of the setup and statistical analysis can be found in appendix D. The precise statistical analysis for SM neutrinos with baselines L_0 corresponding to distances in the solar system can be found in section 4.1. The analysis of astrophysical neutrino sources beyond the solar system can be found in section 4.2. Finally, we consider the influence of a SGWB in section 4.3.

4.1 Neutrinos from within the Solar System

To gain an intuition for the physics involved, we first discuss the simplest yet rather unrealistic scenario of either free falling artificial neutrino sources placed, for example, in a stable Lagrange point within the solar system or neutrinos originating from dark matter decaying or annihilating inside the gravitational potential wells of celestial bodies like the moon. While we will find that neutrinos from farther sources turn out to be more promising for GW detection, the following discussion will help us to identify the challenges to obtain an observable effect. We do not consider solar neutrinos where oscillations are already impeded by strong matter effects. Therefore, we assume an initially pure muon neutrino flux modelled by a Gaussian shaped energy spectrum with a total event count of $N = 10^5$ for an experimental running time of 20 years. We operate within realistically achievable parameter configurations, selecting a neutrino wave packet width in the nm range [50], and conduct a statistical analysis using the parameters in table 1 to verify the estimations from section 3. This enables us to determine the strains and frequencies of GWs to which corresponding experiments would be sensitive to. Figure 4 depicts the results of our analysis for the parameters from table 1 with sensitivity curves for the experiments taken out of reference [51]. LIGO and LIGOa give limits at 90 % CL [52] as well as Virgo [52], and LISA [53]. EPTA, IPTA, and eLISA give limits at 95 % CL [54–56]. In figure 4 we show the upper limit of the strain h as a function

Table 1: Wavelengths λ_{GW} , baselines L_0 , energy ranges E and bin widths ΔE , where effects would be observable for the three chosen GW frequency ranges f_{GW} and neutrino wave packet widths of $\sigma_x = 1$ nm. The oscillation lengths for the different energies are given in table 2.

Scenario	f_{GW}/Hz	$\lambda_{\text{GW}}/\text{km}$	L_0/km	E	ΔE
1				[1, 10]keV	~ 0.45 keV
2	1–10	10^7 – 10^8	$\sim 10^5$	[1, 10]MeV	~ 0.45 MeV
3				[1, 10]GeV	~ 0.45 GeV
4				[1, 10]keV	~ 0.45 keV
5	10^{-6} – 10^{-5}	10^{10} – 10^{11}	$\sim 10^8$	[1, 10]MeV	~ 0.45 MeV
6				[1, 10]GeV	~ 0.45 GeV
7				[1, 10]keV	~ 0.45 keV
8	10^{-9}	10^{17}	$\sim 10^{10}$	[1, 10]MeV	~ 0.45 MeV
9				[1, 10]GeV	~ 0.45 GeV

of the frequency f at 95 % CL assuming the absence of the GW induced decoherence in the experimental data set. It is evident that only three parameter configurations corresponding to the scenarios 2, 6, and 9 from table 1 yield meaningful constraints on the strain h and frequency f of the GW. This is because the condition from equation (16) is not satisfied for the remaining six parameter configurations, and thus, the GW decoherence effect is obfuscated by wavepacket decoherence. Another significant factor at play is the energy binning, which according to equation (17), for example, should be in the meV range for the baseline $L_{0,2}$, which is way smaller than what experiments can resolve.

The sensitivity curves in figure 4 can be divided into two regions: a plateau occurring at frequencies $f \ll L_0^{-1}$ and an oscillatory region at higher frequencies $f \gtrsim L_0^{-1}$. This behavior is understandable when considering equation (10). In the oscillatory region, values of $\tilde{\omega}L_0 = 2\pi k$ with $k \in \mathbb{Z}$ can occur, resulting in $\sin(\tilde{\omega}L_0) = \cos(\tilde{\omega}L_0) - 1 = 0$, and overall no deviation $\Delta L = 0$ from the length L_0 occurs. This behavior can be explained by the fact that at these frequencies, an equal number of wave troughs and wave crests influence the neutrino propagation, leading to no net effect. Hence, this region is not suitable for investigating the parameters of the GW. The most interesting region is the plateau where $fL_0 \ll 1$ holds. Here, $\sin(\tilde{\omega}L_0)/\tilde{\omega}L_0$ approaches one, resulting in a frequency independent amplitude of $\Delta L(t)$ shaping this plateau. Hence, the frequency at which the contour enters the plateau region depends on the baseline L_0 . Furthermore, at the lowest end of the frequency region one can see that the contours transition from a plateau into an oscillating (intermediate) phase. This oscillation is due to the decreasing number of GW cycles $n := \lfloor fT_{\text{exp}} \rfloor$ over which we average the modified flavor transition probability in equation (9). As $n \rightarrow \infty$, i.e. $f \gg T_{\text{exp}}^{-1}$, the contribution of the remaining incomplete period $T_{\text{exp}} - nf$ is negligible compared to the n complete periods. Therefore, the time average corresponds to the average over a single full period. For $n = \mathcal{O}(1)$, i.e. $f \rightarrow T_{\text{exp}}^{-1}$, the suppression of the incomplete cycle becomes weaker resulting in periodically changing weaker or stronger deviations from the flat spacetime predictions, ultimately resulting in the oscillating contour at the lowest frequencies.

According to figure 4, it is possible to achieve constraints on the strain h as low as $h \approx 3.2 \times 10^{-7}$ with scenario 9 from table 1, i.e. SM neutrinos with realistic wave packet widths, and baselines smaller than the diameter of the solar system. These results confirm our prediction from figure 3. Despite these rather weak constraints on the strain h , it is interesting to note that with this method so far unexplored frequency ranges can be probed. An attempt to improve on these sensitivities would require larger wave packet widths σ_x , an approach discussed in Appendix E. Nevertheless, the consideration of neutrinos originating from distances within the solar system poses several challenges. For instance, deploying a detector or the source in a Lagrange point or launching them into the interstellar medium is technologically challenging, to put it mildly. Moreover, even if dark matter exists inside of celestial bodies and decays or annihilates into neutrinos, the corresponding neutrino production regions would be rather large and hence positional averaging would already average out the oscillation pattern and thereby obfuscating the GW induced decoherence effect, c.f. criterion (iv) in section 3.

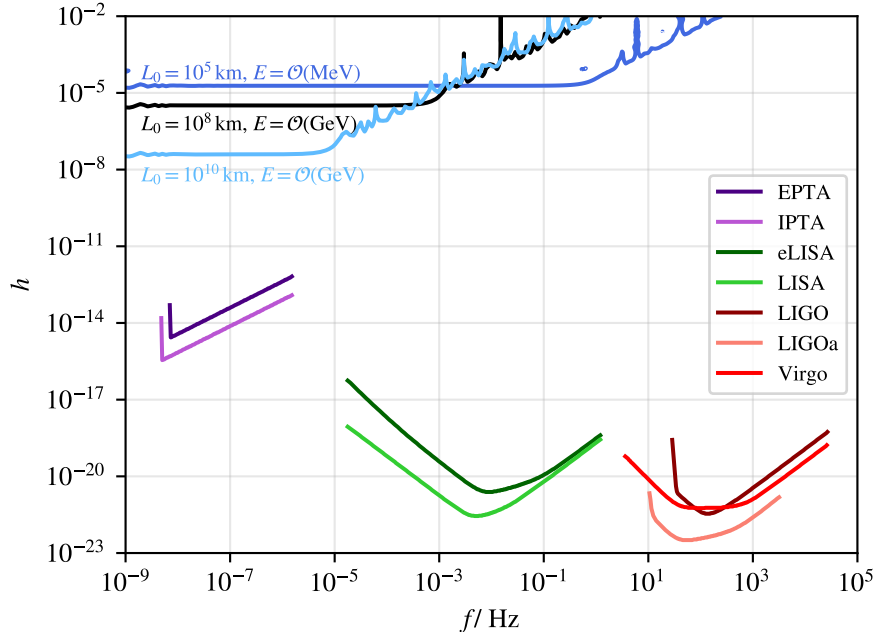


Figure 4: Upper bounds on the GW strain h as a function of the frequency f at 95% confidence level and wave packet widths $\sigma_x = 1$ nm for the scenarios from table 1. We also show the sensitivity curves for EPTA [54], IPTA [55], eLISA [56], LISA [53], LIGO [52], LIGOa [52] and Virgo [52].

Furthermore, matter effects for the propagation out of the core of the celestial bodies have been ignored and finally reasonable wave packet widths yield such weak constraints that this approach is not promising to be investigated further. An alternative option would be a scenario where a hypothetical heavy, sterile neutrino flavor mixes with the active neutrinos. As a consequence of larger mass splitting Δm_{4k}^2 might improve the sensitivity towards smaller strains. We investigate these models in Appendix F, there we also discuss further scenarios. However, due to strong, mass dependent constraints on the sterile-active mixing angles that suppress this oscillation channel, this approach does not provide an advantage over the light neutrino case. Therefore, we turn to the more promising scenario considering neutrinos from outside the solar system.

4.2 Neutrinos from Galactic Pulsars

After pointing out that the prospects to probe GWs at distances within our solar system are rather bleak, we now consider astrophysical neutrino sources outside the solar system. We assume a neutrino flux equivalent to a power-law spectrum $\varphi \propto E^{-2}$ and an initial $(\nu_e, \nu_\mu, \nu_\tau) = (1, 2, 0)$ flavor composition as the commonly considered scenario [57, 58]. We note however, that also different initial flavor ratios are possible depending on the properties and surroundings of the source [59–65].

At these length scales, one challenge lies in the requirement that the neutrino production region needs to be sufficiently small compared to the oscillation length L_{jk}^{osc} , cf. equation (18), in order to detect the decoherence effect caused by GWs. The ratio $L_{jk}^{\text{osc}}/\Sigma_P$ scales linearly with the energy E . Consequently, the higher the energy of the neutrinos, the larger the neutrino production region can be without significantly averaging out the oscillations. Table 2 gives the oscillation lengths, L_{jk}^{osc} , of neutrinos at various energies, E , and thereby provides an intuition about how accurate the region of origin would need to be known.

A possible astrophysical source for neutrinos are supernovae [66], typically emitting MeV neutrinos [67]. However, since we would need to know the location of the neutrino source within a km range to identify decoherence from GWs no sensitivity is expected for such sources, see table 2.

Table 2: Values for the oscillation length L_{jk}^{osc} for different neutrino energies E and mass splitting of $\Delta m_{jk}^2 \sim 10^{-3} \text{ eV}^2$.

E	$L_{jk}^{\text{osc}} / \text{km}$
keV	2.4×10^{-3}
MeV	2.4
GeV	2.4×10^3
TeV	2.4×10^6
PeV	2.4×10^9
EeV	2.4×10^{12}

Another astrophysical source of neutrinos are blazars [68], i.e. active galactic nuclei (AGNs) with jets pointing in our direction. Neutrinos from such a source are expected to be in the energy range from PeV to EeV [69]. According to table 2, for such high-energy neutrinos the spatial size of the neutrino source can be as large as approximately 10^{14} km . While this may be possible for neutrinos produced in the vicinity of a blazar, these sources suffer from an expected low flux of high energy neutrinos reaching the Earth, resulting in a non-significant neutrino count, cf. reference [70], compared to the required event count of $N = 10^4\text{--}10^5$ in our set-up.

Thus, the most promising astrophysical sources of neutrinos are the jets of pulsars [71–81] from our own Galaxy, like for example the Vela ($L_0 = 294_{-50}^{+76} \text{ pc}$ [82]), Crab ($L_0 = 1.9_{-0.18}^{+0.22} \text{ kpc}$ [83]) or Cas A ($L_0 = 3.5 \pm 0.2 \text{ kpc}$ [84]) pulsars. Due to the relatively high expected neutrino fluxes of about $\mathcal{O}(30 \text{ km}^{-2} \text{ yr}^{-1})$, event counts of $N \sim 10^4$ seem to be realistic at future 100 km^2 -neutrino telescopes and a data taking period of about $T_{\text{exp}} \sim 20 \text{ yr}$.

Very high energy neutrinos emerging from pulsars may be generated in two regions: The vicinity of the pulsar’s magnetosphere or in the surrounding pulsar wind nebula. In both cases protons are accelerated to high energies and interact with photons or other protons [71–81, 85, 86] producing pions which in turn decay into neutrinos. So far it is unknown, which of these regions yields the dominant neutrino flux. While the size of the magnetosphere is of the order of several km, depending on the specific properties of the pulsar [85], and thus fulfills the criterion $\Sigma_P \ll L_{jk}^{\text{osc}}$, the pulsar wind nebula is much larger. It is, however, uncertain how large the actual size of the neutrino production region within the nebula really is. In the following, we assume that the width of the production region is sufficiently small compared to the oscillation length, cf. table 2. Even if this assumption does not apply, pulsars remain suitable sources when a potential additional oscillation damping originating from a necessary averaging over the neutrino production region is included in the analysis. Furthermore, we assume neutrino energies in the energy range $E \in [100 \text{ TeV}, 2 \text{ PeV}]$, as predicted e.g. in reference [80], and a linear energy binning of $\Delta E = 95 \text{ TeV}$. With this binning, we conservatively mimic the logarithmic choice of binning used in a recent IceCube analysis of the astrophysical neutrino flux, cf. reference [87]. In the following, we concentrate on neutrinos from the well studied Vela Pulsar, located in the Vela supernova remnant. Figure 5 depicts the the upper limit on the strain h as a function of the frequency f at 95% CL resulting from a statistical analysis for the mentioned parameter configurations. As discussed in the last section, we expect the best sensitivity at $f \ll L_0^{-1}$. At astrophysical distances, like $L_0 \sim 1000 \text{ lyr}$, a new issue arises: In order to achieve a maximum oscillation damping in the time averaged oscillation probability, the averaging interval needs to be of the order of the inverse frequency of the GW, i.e. $T_{\text{exp}} \gtrsim T_{\text{GW}} := f^{-1}$. Since we are mostly interested in $T_{\text{GW}} \gg L_0$ to eliminate a phase dependence completely, we would also need $T_{\text{exp}} \gtrsim T_{\text{GW}} \gg L_0$, corresponding to a 1000 yr period of data taking or more. This is of course impossible to achieve. Nevertheless, a decoherence effect may still be observed given that the neutrino oscillation length is much smaller than the period of the GW, see table 2, albeit with a smaller sensitivity that results from the fact that only a small portion of the GW strain effects the experiment. As a consequence, the contours do not enter

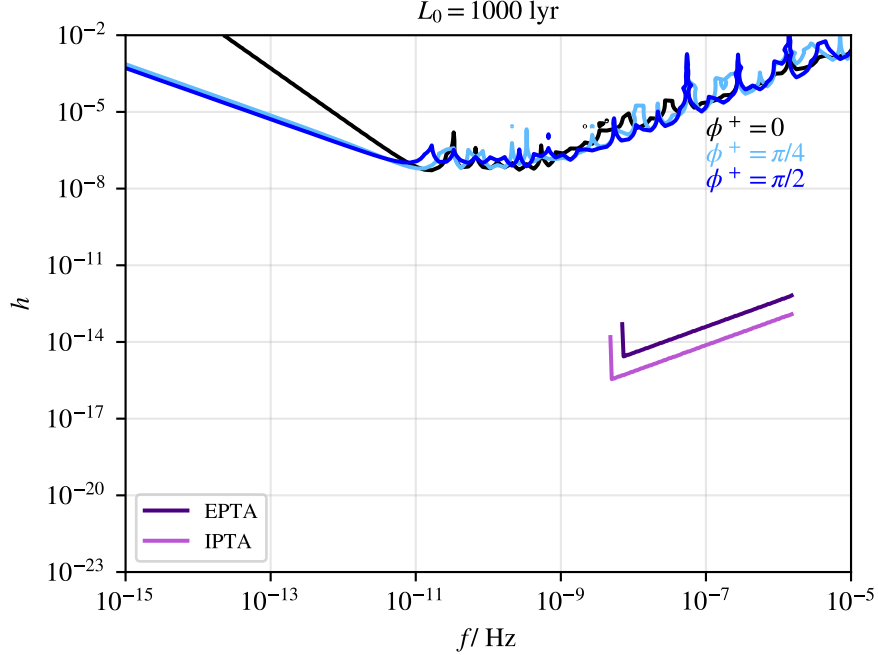


Figure 5: As figure 4, for neutrinos from the Vela Pulsar for different GW phases $\phi^+ \in \{0, \pi/4, \pi/2\}$ and wave packet width $\sigma_x = 1$ nm.

the plateau phase as they would for $T_{\text{exp}} \gg L_0$. Instead the physical length⁴,

$$L(t) = L_0 + \Delta L(t) - \Delta L(0) \stackrel{T_{\text{GW}} \gg L_0 \gg T_{\text{exp}}}{\approx} L_0 \left(1 + \frac{h}{2} \sin(\phi^+) (2\pi ft) + \mathcal{O}\left((2\pi ft)^2\right) \right), \quad (26)$$

approaches the same value, L_0 , as the one used in the flat spacetime prediction as $f \rightarrow 0$. Obviously, due to the lack of averaging over multiple periods of the GW, this method becomes dependent on the initial phase of the GW, ϕ^+ . This behavior can indeed be seen in the contours shown in figure 5 for 20 years of data taking where those upper limits on h for phase shifts closer to $\pi/2$ are stronger than those corresponding to phases closer to zero, cf. equation (26).

Thus, the consideration of neutrinos from pulsars enables us in principle to explore frequency domains below $f \approx 10^{-12}$ Hz, where we expect signals from SMBHBs and EMRIs. However, for SMBHBs, only strains of $h \lesssim 10^{-15}$ [88] and for EMRIs $h \lesssim 10^{-21}$ [51] are expected, which is significantly below the range of $h \approx 10^{-7}$ that can be probed realistically. Besides these expected sources of GW signals in the nHz band neutrino oscillation driven GW detectors would in principle also be sensitive to more exotic models or so-far unknown effects that produce GWs at even lower frequencies below $f_{\text{GW}} \lesssim 10^{-13}$ Hz. Therefore, this method constitutes a complementary approach to the study of anisotropies of the cosmic microwave background [19, 89, 90] in order to probe such low frequency GW signals.

Moreover, at least for approximately plane GW signals, the method described above now depends on the phase of the wave and results in a weaker sensitivity for experimental running times smaller than the equivalent distance between neutrino source and detector. The only way to improve this weak sensitivity is either by taking neutrino data over an unrealistically long time period or by employing various measurements over a very long period.

A more realistic way out of this dilemma exists for another source, the SGWB, a random superposition of low frequency plane wave signals of different phases and directions. Since each neutrino trajectory is perturbed

⁴As discussed in section 2 we need to renormalize $L(t)$ with respect to some time t_0 which we take to be zero for simplicity.

by a slightly different superposition of such waves the effect might become visible even if each signal taken on its own would not lead to a visible effect in the oscillation pattern. We study this effect in more detail in the next section.

A further, common problem with neutrinos from astrophysical sources is the accurate determination of the distance L_0 which is subject to rather large uncertainties compared to the baseline variation caused by the GW. This might also impair the sensitivity to the influence of GW induced decoherence.

4.3 Probing the Stochastic Gravitational Wave Background with Standard Model Neutrinos from Galactic Pulsars

Until now, we considered the interplay of neutrino oscillations and plane GW signals of well defined origin. Another interesting phenomenon can be studied in the nHz frequency band, i.e. the SGWB. In parallel to the recent discovery of the SGWB by PTA collaborations, already several works about possible consequences for neutrino oscillations have appeared [16, 19]. While in these studies the interplay of GW induced decoherence and other sources of oscillation damping was already discussed qualitatively, we now adopt a more quantitative approach by analyzing the scenario considered in reference [19] statistically.

To this end, we revisit equation (1) and incorporate not only the wave packet separation effect into the decoherence term, but also the damping term induced by the SGWB,

$$\mathcal{D}_{jk}(E, L_0) = \left(\frac{L_0}{L_{jk}^{\text{coh}}} \right)^2 + \Gamma_{jk}^{\text{SGWB}}(E). \quad (27)$$

This approach, while being different to the one employed so far, roots in very similar considerations of the modification of the neutrino propagation due to the GW in the density matrix formalism, cf. reference [16] for further details. For the following analysis, we do not average over the running time of the neutrino experiment anymore as we have shown that this effect is negligible at the low GW frequencies of the SGWB. Therefore, we only take into account the stochastic perturbations of the neutrino trajectories caused by an ensemble of GWs through which the neutrino system propagates.

The final expression for $\Gamma_{jk}^{\text{SGWB}}$ according to reference [19] is given by

$$\Gamma_{jk}^{\text{SGWB}} = \frac{3}{64(\gamma - 1)} \left(\frac{|A_*|}{f_{\text{yr}} L_{jk}^{\text{osc}}} \right)^2 \left(\frac{f_{\text{min}}}{f_{\text{yr}}} \right)^{1-\gamma}, \quad (28)$$

where the dependence of the SGWB strain h_c on the frequency f is modelled via a power-law spectrum of the form

$$h_c(f) = A_* \left(\frac{f}{f_{\text{yr}}} \right)^{\frac{3-\gamma}{2}}. \quad (29)$$

Here $f_{\text{yr}} = 1\text{yr}^{-1} \approx 31.7\text{ nHz}$ is the reference frequency, γ is the spectral index, f_{min} is the lowest frequency of the GW spectrum and A_* is the amplitude.

We concentrate on the case of an unspecified source of the SGWB, meaning that A_* as well as the spectral index γ are free parameters for several values of the minimum frequency f_{min} . In the full framework accounting for neutrino wave packet separation as well as finite energy binning, we expect the best results to occur for very high energy neutrinos. This corresponds to those scenarios considered in reference [19] where $f_{\text{min}} \in [10^{-18}, 10^{-15}]$ Hz. For our analysis, we again assume the same setting as in section 4.2, i.e. neutrinos emitted from the Vela Pulsar in the energy range $E \in [100\text{ TeV}, 2\text{ PeV}]$ with a power law flux spectrum $\varphi(E) \propto E^{-2}$. Furthermore, we assume a pure ν_e flux as in reference [19] and wave packet widths of $\sigma_x \sim 1\text{ nm}$.

The results of our analysis are visualized in figure 6. Shown are the 95% confidence level contours of the NLLR function in the γ - A_* plane for different values of minimum frequencies, f_{min} , respectively. The parameter regions to the upper right of these contours are excluded for a data set generated assuming the absence of a GW. For the corresponding configurations, i.e. higher strain and bigger spectral index than indicated by the contour, neutrino oscillations are damped compared to the prediction in flat spacetime. Therefore, our results

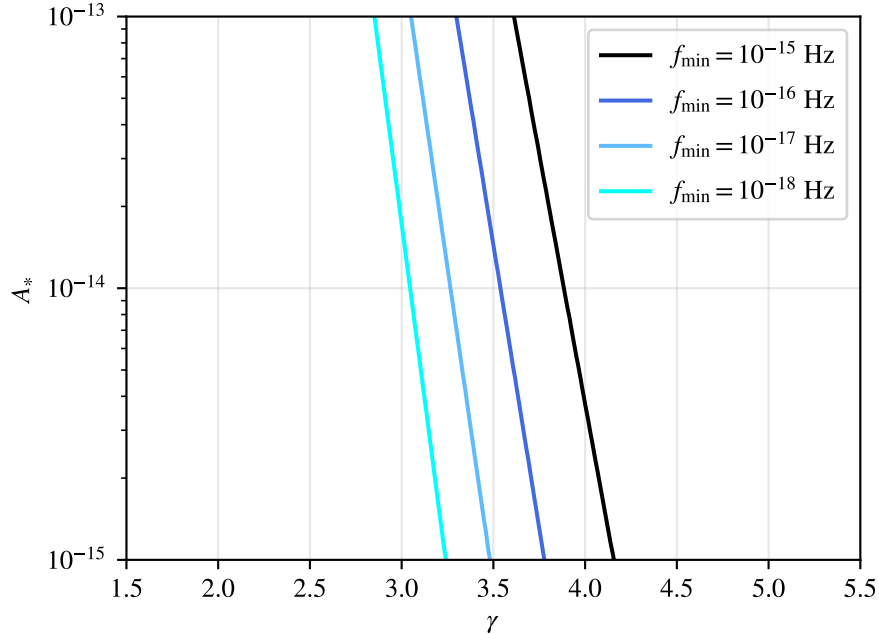


Figure 6: Shown are the limits at 95% CL on the GW amplitude A_* and the spectral index γ for different values of minimum frequencies, $f_{\min} \in \{10^{-18}, 10^{-17}, 10^{-16}, 10^{-15}\}$. Parameter configurations to the upper right of these lines are excluded if the effect of the SGWB is not observed in neutrino oscillation experiments at baselines $L_0 \sim 1000$ lyr, energies $E \in [100 \text{ TeV}, 2 \text{ PeV}]$, bin widths $\Delta E \lesssim 90 \text{ TeV}$ and neutrino wave packet widths $\sigma_x \sim 1 \text{ nm}$.

are in very good agreement with those from reference [19], demonstrating that neutrinos in the PeV energy range can indeed provide new insights to properties of the SGWB, even when taking wave packet decoherence and finite energy resolution of neutrino experiments into account.

For much larger cut-off frequencies like $f_{\min} \in [10^{-12}, 10^{-9}]$ Hz on the other hand, neutrinos with energies in the MeV range would be needed in order to observe a significant effect from the SGWB. A possible source for astrophysical neutrinos of this energy would be supernova neutrinos where typical wave packet widths are $\sigma_x \sim 0.1 \text{ pm}$ [38]. In this case, as discussed in reference [19], decoherence from wave packet separation has already occurred and no effect from the SGWB can be expected unless coherence is restored, e.g. by matter effects in the so called catch-up mechanism [38]. Even if coherence would be restored by any effect, it is questionable, if the neutrino oscillations could be resolved, since that would require an energy resolution or binning of

$$\Delta E \sim 4.17 \times 10^{-12} \left(\frac{10^{-5} \text{ eV}^2}{\Delta m_{jk}^2} \right) \left(\frac{E}{\text{MeV}} \right)^2 \left(\frac{\text{lyr}}{L} \right) \text{ MeV}, \quad (30)$$

cf. equation (17). In addition and as already discussed in section 4.2, uncertainties in the baseline of astrophysical neutrinos can also affect the constraints on GW parameters.

5 Conclusions

In this paper we have studied the influence of a GW signal on neutrino oscillations for a variety of baselines and parameter sets. We have developed a heuristic yet robust model describing the propagation of neutrinos in a spacetime curved by GWs. After pointing out how GWs influence neutrino flavor oscillations by altering the propagation length of neutrinos, we have systematically established conditions under which this effect is

observable. Subsequently, we have performed an NLLR test comparing this effect to the absence of GW induced decoherence in a toy neutrino experiment that allowed us to determine the conditions under which an effect becomes observable. For neutrinos with propagation lengths smaller than the diameter of the solar system, we obtained a sensitivity of $h \approx 10^{-7}$ with realistic wave packet widths of the order 1 nm. For larger wave packet widths we have shown that respective experiments might even reach sensitivities as low as $h \approx 10^{-13}$. While performing experiments within the solar system poses significant challenges, such as placing a neutrino source or detector within a Lagrange point or detecting neutrinos from dark matter decaying in the core of the moon or planets, the situation differs for astrophysical neutrino sources outside the solar system. In particular, we have investigated neutrinos originating from the Vela Pulsar and find a possible sensitivity on GWs ranging from $h \approx 10^{-7}$ to $h \approx 10^{-2}$ in the frequency range of $f \approx 10^{-15}$ to $f \approx 10^{-11}$, which is currently inaccessible by any other experiment. Only significantly weaker bounds from nucleosynthesis exist in this region. For such low frequencies however, the exclusion limits in this case depend on the phase of the GW which impairs the sensitivity to small strains.

Furthermore, we have examined the influence of the SGWB on neutrinos originating from a pulsar, that does not feature the problem of a phase dependent sensitivity, since the neutrino trajectories are altered by a randomly distributed ensemble of GW signals of all phases and directions. We improved on previous investigations of this scenario that have only qualitatively discussed the effect of wave packet decoherence. When considering wave packet decoherence and the finite energy resolution and binning of realistic experiments, we show explicitly that MeV neutrinos are not sensitive to the SGWB, while PeV neutrinos still provide an intriguing possibility to study the SGWB.

In summary, we have discussed how neutrino oscillations are affected by GW signals. Neutrino oscillations provide a promising new avenue to probe the SGWB, while the possibility to detect plane GW signals using neutrino flavor oscillations suffers from relatively low sensitivities especially compared to laser interferometry experiments, which is mostly due to the interplay of the GW induced decoherence effect and other sources of oscillation averaging. Even so, neutrino oscillations may provide a new window in so far unexplored regions of the GW parameter space.

References

- [1] Y. Eroshenko and V. Stasenko, *Symmetry* **15** (2023) no.3, 637 doi:10.3390/sym15030637 [arXiv:2302.05167 [astro-ph.CO]].
- [2] J. Casalderrey-Solana, D. Mateos and M. Sanchez-Garitaonandia, [arXiv:2210.03171 [hep-th]].
- [3] S. Rahvar, *Int. J. Mod. Phys. D* **32** (2023) no.16, 2350103 doi:10.1142/S0218271823501031 [arXiv:2304.00348 [gr-qc]].
- [4] J. Powell, A. Iess, M. Llorens-Monteagudo, M. Obergaulinger, B. Müller, A. Torres-Forné, E. Cuoco and J. A. Font, [arXiv:2311.18221 [astro-ph.HE]].
- [5] A. Eichhorn, R. R. Lino dos Santos and J. L. Miqueleto, *Phys. Rev. D* **109** (2024) no.2, 2 doi:10.1103/PhysRevD.109.026013 [arXiv:2306.17718 [gr-qc]].
- [6] E. Bagui *et al.* [LISA Cosmology Working Group], [arXiv:2310.19857 [astro-ph.CO]].
- [7] M. C. Guzzetti, N. Bartolo, M. Liguori and S. Matarrese, *Riv. Nuovo Cim.* **39** (2016) no.9, 399-495 doi:10.1393/ncr/i2016-10127-1 [arXiv:1605.01615 [astro-ph.CO]].
- [8] G. Agazie *et al.* [NANOGrav], *Astrophys. J. Lett.* **951** (2023) no.1, L8 doi:10.3847/2041-8213/acdac6 [arXiv:2306.16213 [astro-ph.HE]].
- [9] M. Branchesi, M. Maggiore, D. Alonso, C. Badger, B. Banerjee, F. Beirnaert, E. Belgacem, S. Bhagwat, G. Boileau and S. Borhanian, *et al.* *JCAP* **07** (2023), 068 doi:10.1088/1475-7516/2023/07/068 [arXiv:2303.15923 [gr-qc]].

- [10] J. Baker, J. Bellovary, P. L. Bender, E. Berti, R. Caldwell, J. Camp, J. W. Conklin, N. Cornish, C. Cutler and R. DeRosa, *et al.* [arXiv:1907.06482 [astro-ph.IM]].
- [11] B. P. Abbott *et al.* [LIGO Scientific], Rept. Prog. Phys. **72** (2009), 076901 doi:10.1088/0034-4885/72/7/076901 [arXiv:0711.3041 [gr-qc]].
- [12] M. Dvornikov, Phys. Rev. D **100** (2019) no.9, 096014 doi:10.1103/PhysRevD.100.096014 [arXiv:1906.06167 [hep-ph]].
- [13] G. Koutsoumbas and D. Metaxas, Gen. Rel. Grav. **52** (2020) no.10, 102 doi:10.1007/s10714-020-02758-z [arXiv:1909.02735 [hep-ph]].
- [14] M. Dvornikov, J. Phys. Conf. Ser. **1435** (2020) no.1, 012005 doi:10.1088/1742-6596/1435/1/012005 [arXiv:1910.01415 [hep-ph]].
- [15] M. Dvornikov, JCAP **12** (2020), 022 doi:10.1088/1475-7516/2020/12/022 [arXiv:2009.02195 [astro-ph.HE]].
- [16] M. Dvornikov, Phys. Rev. D **104** (2021) no.4, 043018 doi:10.1103/PhysRevD.104.043018 [arXiv:2103.15464 [hep-ph]].
- [17] M. Dvornikov, Moscow Univ. Phys. Bull. **77** (2022) no.2, 439-441 doi:10.3103/S002713492202031X [arXiv:2207.03937 [hep-ph]].
- [18] G. Lambiase, L. Mastrototaro and L. Visinelli, JCAP **01** (2023), 011 doi:10.1088/1475-7516/2023/01/011 [arXiv:2207.08067 [hep-ph]].
- [19] G. Lambiase, L. Mastrototaro and L. Visinelli, Phys. Rev. D **108** (2023) no.12, 123028 doi:10.1103/PhysRevD.108.123028 [arXiv:2306.16977 [astro-ph.HE]].
- [20] A. Domi, T. Eberl, M. J. Fahn, K. Giesel, L. Hennig, U. Katz, R. Kemper and M. Kobler, [arXiv:2403.03106 [gr-qc]].
- [21] S. Mandal, to be published.
- [22] L. Stodolsky, Gen. Rel. Grav. **11** (1979), 391-405 doi:10.1007/BF00759302
- [23] D. Piriz, M. Roy and J. Wudka, Phys. Rev. D **54** (1996), 1587-1599 doi:10.1103/PhysRevD.54.1587 [arXiv:hep-ph/9604403 [hep-ph]].
- [24] D. V. Ahluwalia and C. Burgard, Gen. Rel. Grav. **28** (1996), 1161-1170 doi:10.1007/BF03218936 [arXiv:gr-qc/9603008 [gr-qc]].
- [25] D. V. Ahluwalia and C. Burgard, [arXiv:gr-qc/9606031 [gr-qc]].
- [26] C. Y. Cardall and G. M. Fuller, Phys. Rev. D **55** (1997), 7960-7966 doi:10.1103/PhysRevD.55.7960 [arXiv:hep-ph/9610494 [hep-ph]].
- [27] N. Fornengo, C. Giunti, C. W. Kim and J. Song, Phys. Rev. D **56** (1997), 1895-1902 doi:10.1103/PhysRevD.56.1895 [arXiv:hep-ph/9611231 [hep-ph]].
- [28] G. Lambiase, G. Papini, R. Punzi and G. Scarpetta, Phys. Rev. D **71** (2005), 073011 doi:10.1103/PhysRevD.71.073011 [arXiv:gr-qc/0503027 [gr-qc]].
- [29] L. Visinelli, Gen. Rel. Grav. **47** (2015) no.5, 62 doi:10.1007/s10714-015-1899-z [arXiv:1410.1523 [gr-qc]].
- [30] B. Kayser, Phys. Rev. D **24** (1981), 110 doi:10.1103/PhysRevD.24.110
- [31] P. H. Frampton and P. Vogel, Phys. Rept. **82** (1982), 339-388 doi:10.1016/0370-1573(82)90159-4
- [32] C. Giunti, C. W. Kim and U. W. Lee, Phys. Rev. D **44** (1991), 3635-3640 doi:10.1103/PhysRevD.44.3635

- [33] C. Giunti, C. W. Kim, J. A. Lee and U. W. Lee, Phys. Rev. D **48** (1993), 4310-4317 doi:10.1103/PhysRevD.48.4310 [arXiv:hep-ph/9305276 [hep-ph]].
- [34] C. Giunti, C. W. Kim and U. W. Lee, Phys. Lett. B **421** (1998), 237-244 doi:10.1016/S0370-2693(98)00014-8 [arXiv:hep-ph/9709494 [hep-ph]].
- [35] K. Kiers and N. Weiss, Phys. Rev. D **57** (1998), 3091-3105 doi:10.1103/PhysRevD.57.3091 [arXiv:hep-ph/9710289 [hep-ph]].
- [36] E. K. Akhmedov and A. Y. Smirnov, Phys. Atom. Nucl. **72** (2009), 1363-1381 doi:10.1134/S1063778809080122 [arXiv:0905.1903 [hep-ph]].
- [37] E. Akhmedov, J. Kopp and M. Lindner, [arXiv:1405.7275 [hep-ph]].
- [38] J. Kersten and A. Y. Smirnov, Eur. Phys. J. C **76** (2016) no.6, 339 doi:10.1140/epjc/s10052-016-4187-5 [arXiv:1512.09068 [hep-ph]].
- [39] E. Akhmedov, J. Kopp and M. Lindner, JCAP **09** (2017), 017 doi:10.1088/1475-7516/2017/09/017 [arXiv:1702.08338 [hep-ph]].
- [40] D. V. Naumov and V. A. Naumov, Phys. Part. Nucl. **51** (2020) no.1, 1-106 doi:10.1134/S1063779620010050
- [41] R. L. Workman *et al.* [Particle Data Group], PTEP **2022** (2022), 083C01 doi:10.1093/ptep/ptac097
- [42] B. P. Abbott *et al.* [LIGO Scientific and Virgo], Phys. Rev. Lett. **116** (2016) no.6, 061102 doi:10.1103/PhysRevLett.116.061102 [arXiv:1602.03837 [gr-qc]].
- [43] C. A. Argüelles, T. Bertólez-Martínez and J. Salvado, Phys. Rev. D **107** (2023) no.3, 036004 doi:10.1103/PhysRevD.107.036004 [arXiv:2201.05108 [hep-ph]].
- [44] J. Antoniadis *et al.* [EPTA], Astron. Astrophys. **678** (2023), A48 doi:10.1051/0004-6361/202346841 [arXiv:2306.16224 [astro-ph.HE]].
- [45] G. Agazie *et al.* [NANOGrav], Astrophys. J. Lett. **951** (2023) no.1, L9 doi:10.3847/2041-8213/acda9a [arXiv:2306.16217 [astro-ph.HE]].
- [46] B. P. Abbott, R. Abbott, T. D. Abbott, C. Adams, R. X. Adhikari, R. A. Anderson, S. B. Anderson, K. Arai, M. A. Arain and S. M. Aston, *et al.* Phys. Rev. D **93** (2016) no.11, 112004 doi:10.1103/PhysRevD.93.112004 [arXiv:1604.00439 [astro-ph.IM]].
- [47] A. Sesana, Class. Quant. Grav. **30** (2013), 244009 doi:10.1088/0264-9381/30/24/244009 [arXiv:1307.4086 [astro-ph.CO]].
- [48] C. Q. Ye, H. M. Fan, A. Torres-Orjuela, J. d. Zhang and Y. M. Hu, [arXiv:2310.03520 [gr-qc]].
- [49] S. Chen, A. Sesana and C. J. Conelice, Mon. Not. Roy. Astron. Soc. **488** (2019) no.1, 401-418 doi:10.1093/mnras/stz1722 [arXiv:1810.04184 [astro-ph.GA]].
- [50] F. P. An *et al.* [Daya Bay], Eur. Phys. J. C **77** (2017) no.9, 606 doi:10.1140/epjc/s10052-017-4970-y [arXiv:1608.01661 [hep-ex]].
- [51] C. J. Moore, R. H. Cole and C. P. L. Berry, Class. Quant. Grav. **32** (2015) no.1, 015014 doi:10.1088/0264-9381/32/1/015014 [arXiv:1408.0740 [gr-qc]].
- [52] J. Abadie *et al.* [LIGO Scientific and VIRGO], Phys. Rev. D **81** (2010), 102001 doi:10.1103/PhysRevD.81.102001 [arXiv:1002.1036 [gr-qc]].
- [53] B. S. Sathyaprakash and B. F. Schutz, Living Rev. Rel. **12** (2009), 2 doi:10.12942/lrr-2009-2 [arXiv:0903.0338 [gr-qc]].

- [54] M. Kramer *et al.* [EPTA], *Class. Quant. Grav.* **30** (2013), 224009 doi:10.1088/0264-9381/30/22/224009
- [55] J. Antoniadis, Z. Arzoumanian, S. Babak, M. Bailes, A. S. B. Nielsen, P. T. Baker, C. G. Bassa, B. Bercsy, A. Berthreau and M. Bonetti, *et al.* *Mon. Not. Roy. Astron. Soc.* **510** (2022) no.4, 4873-4887 doi:10.1093/mnras/stab3418 [arXiv:2201.03980 [astro-ph.HE]].
- [56] P. Amaro-Seoane, S. Aoudia, S. Babak, P. Binétruy, E. Berti, A. Bohe, C. Caprini, M. Colpi, N. J. Cornish and K. Danzmann, *et al.* *GW Notes* **6** (2013), 4-110 [arXiv:1201.3621 [astro-ph.CO]].
- [57] J. F. Beacom, N. F. Bell, D. Hooper, S. Pakvasa and T. J. Weiler, *Phys. Rev. D* **68** (2003), 093005 [erratum: *Phys. Rev. D* **72** (2005), 019901] doi:10.1103/PhysRevD.68.093005 [arXiv:hep-ph/0307025 [hep-ph]].
- [58] H. Athar, C. S. Kim and J. Lee, *Mod. Phys. Lett. A* **21** (2006), 1049-1066 doi:10.1142/S021773230602038X [arXiv:hep-ph/0505017 [hep-ph]].
- [59] J. P. Rachen and P. Meszaros, *Phys. Rev. D* **58** (1998), 123005 doi:10.1103/PhysRevD.58.123005 [arXiv:astro-ph/9802280 [astro-ph]].
- [60] L. A. Anchordoqui, H. Goldberg, F. Halzen and T. J. Weiler, *Phys. Lett. B* **593** (2004), 42 doi:10.1016/j.physletb.2004.04.054 [arXiv:astro-ph/0311002 [astro-ph]].
- [61] T. Kashti and E. Waxman, *Phys. Rev. Lett.* **95** (2005), 181101 doi:10.1103/PhysRevLett.95.181101 [arXiv:astro-ph/0507599 [astro-ph]].
- [62] M. Kachelrieß and R. Tomàs, *Phys. Rev. D* **74** (2006), 063009 doi:10.1103/PhysRevD.74.063009
- [63] P. Lipari, M. Lusignoli and D. Meloni, *Phys. Rev. D* **75** (2007), 123005 doi:10.1103/PhysRevD.75.123005 [arXiv:0704.0718 [astro-ph]].
- [64] S. R. Klein, R. E. Mikkelsen and J. Becker Tjus, *Astrophys. J.* **779** (2013), 106 doi:10.1088/0004-637X/779/2/106 [arXiv:1208.2056 [astro-ph.HE]].
- [65] M. Bustamante, J. F. Beacom and W. Winter, *Phys. Rev. Lett.* **115** (2015) no.16, 161302 doi:10.1103/PhysRevLett.115.161302 [arXiv:1506.02645 [astro-ph.HE]].
- [66] H. T. Janka, doi:10.1007/978-3-319-21846-5_4 [arXiv:1702.08713 [astro-ph.HE]].
- [67] A. M. Suliga, doi:10.1007/978-981-15-8818-1_129-1 [arXiv:2207.09632 [astro-ph.HE]].
- [68] F. Oikonomou, *PoS ICRC2021* (2022), 030 doi:10.22323/1.395.0030 [arXiv:2201.05623 [astro-ph.HE]].
- [69] M. Boettcher, M. Fu, T. Govenor, Q. King and P. Roustazadeh, *Acta Phys. Polon. Supp.* **15** (2022) no.3, 8 doi:10.5506/APhysPolBSupp.15.3-A8 [arXiv:2204.12242 [astro-ph.HE]].
- [70] F. Oikonomou, K. Murase, P. Padovani, E. Resconi and P. Mészáros, *Mon. Not. Roy. Astron. Soc.* **489** (2019) no.3, 4347-4366 doi:10.1093/mnras/stz2246 [arXiv:1906.05302 [astro-ph.HE]].
- [71] R. J. Protheroe, W. Bednarek and Q. Luo, *Astropart. Phys.* **9** (1998), 1-14 doi:10.1016/S0927-6505(98)00014-0 [arXiv:astro-ph/9703045 [astro-ph]].
- [72] R. Gandhi, *Nucl. Phys. B Proc. Suppl.* **91** (2001), 453-461 doi:10.1016/S0920-5632(00)00975-0 [arXiv:hep-ph/0011176 [hep-ph]].
- [73] J. H. Beall and W. Bednarek, *Astrophys. J.* **569** (2002), 343-348 doi:10.1086/339276 [arXiv:astro-ph/0108447 [astro-ph]].
- [74] D. Guetta and E. Amato, *Astropart. Phys.* **19** (2003), 403-407 doi:10.1016/S0927-6505(02)00221-9 [arXiv:astro-ph/0209537 [astro-ph]].

- [75] D. Guetta and J. Granot, Phys. Rev. Lett. **90** (2003), 201103 doi:10.1103/PhysRevLett.90.201103 [arXiv:astro-ph/0212045 [astro-ph]].
- [76] S. Razzaque, P. Meszaros and E. Waxman, Phys. Rev. Lett. **90** (2003), 241103 doi:10.1103/PhysRevLett.90.241103 [arXiv:astro-ph/0212536 [astro-ph]].
- [77] C. D. Dermer and A. Atoyan, Phys. Rev. Lett. **91** (2003), 071102 doi:10.1103/PhysRevLett.91.071102 [arXiv:astro-ph/0301030 [astro-ph]].
- [78] W. Bednarek, Astron. Astrophys. **407** (2003), 1-6 doi:10.1051/0004-6361:20030929 [arXiv:astro-ph/0305430 [astro-ph]].
- [79] B. Link and F. Burgio, Phys. Rev. Lett. **94** (2005), 181101 doi:10.1103/PhysRevLett.94.181101 [arXiv:astro-ph/0412520 [astro-ph]].
- [80] B. Link and F. Burgio, Mon. Not. Roy. Astron. Soc. **371** (2006), 375-379 doi:10.1111/j.1365-2966.2006.10665.x [arXiv:astro-ph/0604379 [astro-ph]].
- [81] K. Fang, JCAP **06** (2015), 004 doi:10.1088/1475-7516/2015/06/004 [arXiv:1411.2174 [astro-ph.HE]].
- [82] P. A. Caraveo, A. De Luca, R. P. Mignani and G. F. Bignami, Astrophys. J. **561** (2001), 930 doi:10.1086/323377 [arXiv:astro-ph/0107282 [astro-ph]].
- [83] R. Lin, M. H. van Kerkwijk, F. Kirsten, U. L. Pen and A. T. Deller, Astrophys. J. **952** (2023) no.2, 161 doi:10.3847/1538-4357/acdc98 [arXiv:2306.01617 [astro-ph.HE]].
- [84] G. G. Pavlov, D. Sanwal and M. A. Teter, IAU Symp. **218** (2004), 239 [arXiv:astro-ph/0311526 [astro-ph]].
- [85] C. Guépin, B. Cerutti and K. Kotera, Astron. Astrophys. **635** (2020), A138 doi:10.1051/0004-6361/201936816 [arXiv:1910.11387 [astro-ph.HE]].
- [86] A. Asthana, A. A. Mushtukov, A. A. Dobrynina and I. S. Ognev, Mon. Not. Roy. Astron. Soc. **522** (2023) no.3, 3405-3411 doi:10.1093/mnras/stad1118 [arXiv:2304.04520 [astro-ph.HE]].
- [87] R. Abbasi, M. Ackermann, J. Adams, S. K. Agarwalla, J. A. Aguilar, M. Ahlers, J. M. Alameddine, N. M. Amin, K. Andeen and G. Anton, *et al.* [arXiv:2402.18026 [astro-ph.HE]].
- [88] R. M. Shannon, V. Ravi, W. A. Coles, G. Hobbs, M. J. Keith, R. N. Manchester, J. S. B. Wyithe, M. Bailes, N. D. R. Bhat and S. Burke-Spolaor, *et al.* Science **342** (2013) no.6156, 334-337 doi:10.1126/science.1238012 [arXiv:1310.4569 [astro-ph.CO]].
- [89] L. M. Krauss and M. J. White, Phys. Rev. Lett. **69** (1992), 869-872 doi:10.1103/PhysRevLett.69.869 [arXiv:hep-ph/9205212 [hep-ph]].
- [90] K. S. Thorne, [arXiv:gr-qc/9506086 [gr-qc]].
- [91] P. D. Bolton, F. F. Deppisch and P. S. Bhupal Dev, JHEP **03** (2020), 170 doi:10.1007/JHEP03(2020)170 [arXiv:1912.03058 [hep-ph]].
- [92] J. M. Berryman, Phys. Rev. D **100** (2019) no.2, 023540 doi:10.1103/PhysRevD.100.023540 [arXiv:1905.03254 [hep-ph]].
- [93] I. Alekseev *et al.* [DANSS], Phys. Lett. B **787** (2018), 56-63 doi:10.1016/j.physletb.2018.10.038 [arXiv:1804.04046 [hep-ex]].
- [94] M. Cirelli, G. Marandella, A. Strumia and F. Vissani, Nucl. Phys. B **708** (2005), 215-267 doi:10.1016/j.nuclphysb.2004.11.056 [arXiv:hep-ph/0403158 [hep-ph]].
- [95] M. Dentler, Á. Hernández-Cabezudo, J. Kopp, P. A. N. Machado, M. Maltoni, I. Martinez-Soler and T. Schwetz, JHEP **08** (2018), 010 doi:10.1007/JHEP08(2018)010 [arXiv:1803.10661 [hep-ph]].

- [96] Y. J. Ko *et al.* [NEOS], Phys. Rev. Lett. **118** (2017) no.12, 121802 doi:10.1103/PhysRevLett.118.121802 [arXiv:1610.05134 [hep-ex]].
- [97] K. H. Hiddemann, H. Daniel and O. Schwentker, J. Phys. G **21** (1995), 639-650 doi:10.1088/0954-3899/21/5/008
- [98] C. Kraus, A. Singer, K. Valerius and C. Weinheimer, Eur. Phys. J. C **73** (2013) no.2, 2323 doi:10.1140/epjc/s10052-013-2323-z [arXiv:1210.4194 [hep-ex]].
- [99] A. I. Belesev, A. I. Berlev, E. V. Geraskin, A. A. Golubev, N. A. Likhovid, A. A. Nozik, V. S. Pantuev, V. I. Parfenov and A. K. Skasyrskaya, J. Phys. G **41** (2014), 015001 doi:10.1088/0954-3899/41/1/015001 [arXiv:1307.5687 [hep-ex]].
- [100] J. N. Abdurashitov, A. I. Belesev, V. G. Chernov, E. V. Geraskin, A. A. Golubev, P. V. Grigorieva, G. A. Koroteev, N. A. Likhovid, A. A. Nozik and V. S. Pantuev, *et al.* Pisma Zh. Eksp. Teor. Fiz. **105** (2017) no.12, 723-724 doi:10.1134/S0021364017120013 [arXiv:1703.10779 [hep-ex]].
- [101] E. Holzschuh, W. Kundig, L. Palermo, H. Stussi and P. Wenk, Phys. Lett. B **451** (1999), 247-255 doi:10.1016/S0370-2693(99)00200-2
- [102] E. Holzschuh, L. Palermo, H. Stussi and P. Wenk, Phys. Lett. B **482** (2000), 1-9 doi:10.1016/S0370-2693(00)00476-7
- [103] A. V. Derbin, A. I. Egorov, S. V. Bakhlanov and V. N. Muratova, JETP Lett. **66** (1997), 88-92 doi:10.1134/1.567508
- [104] K. Schreckenbach, G. Colvin and F. Von Feilitzsch, Phys. Lett. B **129** (1983), 265-268 doi:10.1016/0370-2693(83)90858-4
- [105] S. Friedrich, G. B. Kim, C. Bray, R. Cantor, J. Dilling, S. Fretwell, J. A. Hall, A. Lennarz, V. Lordi and P. Machule, *et al.* Phys. Rev. Lett. **126** (2021) no.2, 021803 doi:10.1103/PhysRevLett.126.021803 [arXiv:2010.09603 [nucl-ex]].
- [106] A. Aguilar-Arevalo *et al.* [PIENU], Phys. Rev. D **97** (2018) no.7, 072012 doi:10.1103/PhysRevD.97.072012 [arXiv:1712.03275 [hep-ex]].
- [107] D. A. Bryman and R. Shrock, Phys. Rev. D **100** (2019) no.5, 053006 doi:10.1103/PhysRevD.100.053006 [arXiv:1904.06787 [hep-ph]].
- [108] D. A. Bryman and R. Shrock, Phys. Rev. D **100** (2019), 073011 doi:10.1103/PhysRevD.100.073011 [arXiv:1909.11198 [hep-ph]].
- [109] G. Bernardi, G. Carugno, J. Chauveau, F. Dicarolo, M. Dris, J. Dumarchez, M. Ferro-Luzzi, J. M. Levy, D. Lukas and J. M. Perreau, *et al.* Phys. Lett. B **203** (1988), 332-334 doi:10.1016/0370-2693(88)90563-1
- [110] S. A. Baranov, Y. A. Batusov, A. A. Borisov, S. A. Bunyatov, V. Y. Valuev, A. S. Vovenko, V. N. Goryachev, M. M. Kirsanov, D. Kish and O. L. Klimov, *et al.* Phys. Lett. B **302** (1993), 336-340 doi:10.1016/0370-2693(93)90405-7
- [111] E. Cortina Gil *et al.* [NA62], Phys. Lett. B **807** (2020), 135599 doi:10.1016/j.physletb.2020.135599 [arXiv:2005.09575 [hep-ex]].
- [112] K. Abe *et al.* [T2K], Phys. Rev. D **100** (2019) no.5, 052006 doi:10.1103/PhysRevD.100.052006 [arXiv:1902.07598 [hep-ex]].
- [113] K. Abe *et al.* [Super-Kamiokande], Phys. Rev. D **91** (2015), 052019 doi:10.1103/PhysRevD.91.052019 [arXiv:1410.2008 [hep-ex]].

- [114] S. Kovalenko, Z. Lu and I. Schmidt, Phys. Rev. D **80** (2009), 073014 doi:10.1103/PhysRevD.80.073014 [arXiv:0907.2533 [hep-ph]].
- [115] A. Atre, T. Han, S. Pascoli and B. Zhang, JHEP **05** (2009), 030 doi:10.1088/1126-6708/2009/05/030 [arXiv:0901.3589 [hep-ph]].
- [116] J. C. Helo, S. Kovalenko and I. Schmidt, Nucl. Phys. B **853** (2011), 80-104 doi:10.1016/j.nuclphysb.2011.07.020 [arXiv:1005.1607 [hep-ph]].
- [117] A. Abada, V. De Romeri, M. Lucente, A. M. Teixeira and T. Toma, JHEP **02** (2018), 169 doi:10.1007/JHEP02(2018)169 [arXiv:1712.03984 [hep-ph]].
- [118] F. Bergsma *et al.* [CHARM], Phys. Lett. B **166** (1986), 473-478 doi:10.1016/0370-2693(86)91601-1
- [119] P. Vilain *et al.* [CHARM II], Phys. Lett. B **343** (1995), 453-458 doi:10.1016/0370-2693(94)01422-9
- [120] R. Barouki, G. Marocco and S. Sarkar, SciPost Phys. **13** (2022), 118 doi:10.21468/SciPostPhys.13.5.118 [arXiv:2208.00416 [hep-ph]].
- [121] M. Ablikim *et al.* [BESIII], Phys. Rev. D **99** (2019) no.11, 112002 doi:10.1103/PhysRevD.99.112002 [arXiv:1902.02450 [hep-ex]].
- [122] J. Badier *et al.* [NA3], Z. Phys. C **31** (1986), 21 doi:10.1007/BF01559588
- [123] D. Liventsev *et al.* [Belle], Phys. Rev. D **87** (2013) no.7, 071102 [erratum: Phys. Rev. D **95** (2017) no.9, 099903] doi:10.1103/PhysRevD.87.071102 [arXiv:1301.1105 [hep-ex]].
- [124] P. Abreu *et al.* [DELPHI], Z. Phys. C **74** (1997), 57-71 [erratum: Z. Phys. C **75** (1997), 580] doi:10.1007/s002880050370
- [125] O. Adriani *et al.* [L3], Phys. Lett. B **295** (1992), 371-382 doi:10.1016/0370-2693(92)91579-X
- [126] P. Achard *et al.* [L3], Phys. Lett. B **517** (2001), 67-74 doi:10.1016/S0370-2693(01)00993-5 [arXiv:hep-ex/0107014 [hep-ex]].
- [127] G. Aad *et al.* [ATLAS], JHEP **07** (2015), 162 doi:10.1007/JHEP07(2015)162 [arXiv:1506.06020 [hep-ex]].
- [128] G. Aad *et al.* [ATLAS], JHEP **10** (2019), 265 doi:10.1007/JHEP10(2019)265 [arXiv:1905.09787 [hep-ex]].
- [129] A. M. Sirunyan *et al.* [CMS], JHEP **01** (2019), 122 doi:10.1007/JHEP01(2019)122 [arXiv:1806.10905 [hep-ex]].
- [130] A. M. Sirunyan *et al.* [CMS], Phys. Rev. Lett. **120** (2018) no.22, 221801 doi:10.1103/PhysRevLett.120.221801 [arXiv:1802.02965 [hep-ex]].
- [131] A. Das, P. S. B. Dev and C. S. Kim, Phys. Rev. D **95** (2017) no.11, 115013 doi:10.1103/PhysRevD.95.115013 [arXiv:1704.00880 [hep-ph]].
- [132] M. Blennow, P. Coloma, E. Fernandez-Martinez, J. Hernandez-Garcia and J. Lopez-Pavon, JHEP **04** (2017), 153 doi:10.1007/JHEP04(2017)153 [arXiv:1609.08637 [hep-ph]].
- [133] F. del Aguila, J. de Blas and M. Perez-Victoria, Phys. Rev. D **78** (2008), 013010 doi:10.1103/PhysRevD.78.013010 [arXiv:0803.4008 [hep-ph]].
- [134] J. de Blas, EPJ Web Conf. **60** (2013), 19008 doi:10.1051/epjconf/20136019008 [arXiv:1307.6173 [hep-ph]].
- [135] S. Antusch and O. Fischer, JHEP **10** (2014), 094 doi:10.1007/JHEP10(2014)094 [arXiv:1407.6607 [hep-ph]].
- [136] S. Bridle, J. Elvin-Poole, J. Evans, S. Fernandez, P. Guzowski and S. Soldner-Rembold, Phys. Lett. B **764** (2017), 322-327 doi:10.1016/j.physletb.2016.11.050 [arXiv:1607.00032 [astro-ph.CO]].

- [137] A. C. Vincent, E. F. Martinez, P. Hernández, M. Lattanzi and O. Mena, *JCAP* **04** (2015), 006 doi:10.1088/1475-7516/2015/04/006 [arXiv:1408.1956 [astro-ph.CO]].
- [138] A. Boyarsky, O. Ruchayskiy and M. Shaposhnikov, *Ann. Rev. Nucl. Part. Sci.* **59** (2009), 191-214 doi:10.1146/annurev.nucl.010909.083654 [arXiv:0901.0011 [hep-ph]].
- [139] O. Ruchayskiy and A. Ivashko, *JCAP* **10** (2012), 014 doi:10.1088/1475-7516/2012/10/014 [arXiv:1202.2841 [hep-ph]].
- [140] K. C. Y. Ng, B. M. Roach, K. Perez, J. F. Beacom, S. Horiuchi, R. Krivonos and D. R. Wik, *Phys. Rev. D* **99** (2019), 083005 doi:10.1103/PhysRevD.99.083005 [arXiv:1901.01262 [astro-ph.HE]].
- [141] B. M. Roach, K. C. Y. Ng, K. Perez, J. F. Beacom, S. Horiuchi, R. Krivonos and D. R. Wik, *Phys. Rev. D* **101** (2020) no.10, 103011 doi:10.1103/PhysRevD.101.103011 [arXiv:1908.09037 [astro-ph.HE]].
- [142] X. Shi and G. Sigl, *Phys. Lett. B* **323** (1994), 360-366 [erratum: *Phys. Lett. B* **324** (1994), 516-516] doi:10.1016/0370-2693(94)91232-7 [arXiv:hep-ph/9312247 [hep-ph]].
- [143] G. G. Raffelt and S. Zhou, *Phys. Rev. D* **83** (2011), 093014 doi:10.1103/PhysRevD.83.093014 [arXiv:1102.5124 [hep-ph]].
- [144] S. Zhou, *Int. J. Mod. Phys. A* **30** (2015) no.13, 1530033 doi:10.1142/S0217751X15300331 [arXiv:1504.02729 [hep-ph]].
- [145] H. Nunokawa, J. T. Peltoniemi, A. Rossi and J. W. F. Valle, *Phys. Rev. D* **56** (1997), 1704-1713 doi:10.1103/PhysRevD.56.1704 [arXiv:hep-ph/9702372 [hep-ph]].
- [146] M. Galeazzi, F. Fontanelli, F. Gatti and S. Vitale, *Phys. Rev. Lett.* **86** (2001), 1978-1981 doi:10.1103/PhysRevLett.86.1978
- [147] F. P. Calaprice and D. J. Millener, *Phys. Rev. C* **27** (1983), 1175-1181 doi:10.1103/PhysRevC.27.1175
- [148] A. I. Derbin, A. V. Chernyi, L. A. Popeko, V. N. Muratova, G. A. Shishkina and S. I. Bakhlanov, *JETP Lett.* **57** (1993), 768-772
- [149] C. Hagner, M. Altmann, F. von Feilitzsch, L. Oberauer, Y. Declais and E. Kajfasz, *Phys. Rev. D* **52** (1995), 1343-1352 doi:10.1103/PhysRevD.52.1343
- [150] G. Bellini *et al.* [Borexino], *Phys. Rev. D* **88** (2013) no.7, 072010 doi:10.1103/PhysRevD.88.072010 [arXiv:1311.5347 [hep-ex]].

A Geodesics in Gravitational Wave Spacetimes: The Boundary Value Problem

Within our heuristic approach, we replace the baseline with a modified length, as it is subject to the effects of GW as can be seen in equation (4). In order to calculate this spatial length, we first rewrite equation (4) by using the on-shell condition

$$1 = g_{\mu\nu} \dot{\gamma}^\mu \dot{\gamma}^\nu \quad (31)$$

$$\Leftrightarrow 1 = (\dot{\gamma}^0)^2 + g_{jk} \dot{\gamma}^j \dot{\gamma}^k \quad (32)$$

$$\Leftrightarrow -g_{jk} \dot{\gamma}^j \dot{\gamma}^k = (\dot{\gamma}^0)^2 - 1. \quad (33)$$

Here we furthermore employed the transverse traceless (TT) gauge implying $g_{j0} \equiv 0$ and $g_{00} \equiv 1$ in our convention. Substituting this result into equation (4) yields

$$L = \int_{\tau_P}^{\tau_D} \left((\dot{\gamma}^0)^2 - 1 \right)^{\frac{1}{2}} d\tau. \quad (34)$$

To calculate this modification, it is initially necessary to compute the neutrino geodesic in our GW spacetime. To this end, we solve the geodesic equation for given boundary conditions (BC), i.e.

$$\ddot{\gamma}^\mu(\tau) = -\Gamma_{\alpha\beta}^\mu(\gamma(\tau)) \dot{\gamma}^\alpha(\tau) \dot{\gamma}^\beta(\tau), \quad (35)$$

$$\gamma^\alpha(\tau_P) = X_P^\alpha, \quad (36)$$

$$\gamma^\alpha(\tau_D) = X_D^\alpha. \quad (37)$$

Since our metric is close to $\eta = \text{diag}(1, -1, -1, -1)$, we adopt the ansatz

$$\gamma^\alpha(\tau) = \gamma_0^\alpha(\tau) + \epsilon \Delta \gamma^\alpha(\tau). \quad (38)$$

In general the boundary value problem (BVP) of the geodesic equation is not well posed for arbitrarily far separated production and detection points since there may be more than one shortest curve connecting these points. In our specific scenario, however, we assume that geodesics between two points are inherently unique because our spacetime closely resembles Minkowski spacetime.

Upon substituting this ansatz into the geodesic equation, we obtain, keeping only terms up to first order in ϵ ,

$$\ddot{\gamma}_0^\mu(\tau) + \epsilon \Delta \ddot{\gamma}^\mu(\tau) \approx -\frac{\epsilon}{2} \eta^{\mu\nu} (\partial_\alpha h_{\nu\beta} + \partial_\beta h_{\nu\alpha} - \partial_\nu h_{\alpha\beta}) |_{\gamma_0(\tau)} \dot{\gamma}_0^\alpha \dot{\gamma}_0^\beta. \quad (39)$$

By matching terms of the same order in ϵ we arrive at the following set of equations:

$$\ddot{\gamma}_0^\mu(\tau) = 0, \quad (40)$$

$$\Delta \ddot{\gamma}^\mu(\tau) = -\frac{\eta^{\mu\nu}}{2} (\partial_\alpha h_{\nu\beta} + \partial_\beta h_{\nu\alpha} - \partial_\nu h_{\alpha\beta}) |_{\gamma_0(\tau)} \dot{\gamma}_0^\alpha \dot{\gamma}_0^\beta. \quad (41)$$

Equation (40) is easily solved by $\gamma_0^\mu(\lambda) = a^\mu + \lambda u^\mu$. Using our BC from above (at zeroth order in ϵ) on the flat spacetime part of the geodesic, the constants of integration can be determined to yield

$$\gamma_0^\mu(\tau) = X_P^\mu + (\tau - \tau_P) u^\mu, \quad (42)$$

where $u^\mu = (X_D^\mu - X_P^\mu)/(\tau_D - \tau_P)$. For the geodesic correction $\Delta\gamma$, we hence obtain the differential equation

$$\Delta \ddot{\gamma}^\mu(\tau) = -\frac{\eta^{\mu\nu}}{2} (2\partial_\alpha h_{\nu\beta} - \partial_\nu h_{\alpha\beta}) |_{\gamma_0(\tau)} u^\alpha u^\beta =: \Delta a^\mu(\tau), \quad (43)$$

and BC, $\Delta\gamma(\tau_P) = \Delta\gamma(\tau_D) = 0$, at first order in ϵ . Integrating $\Delta\ddot{\gamma}^\mu(\tau)$ leads to the correction to the four velocity, i.e.

$$\Delta \dot{\gamma}^\mu(\tau) = \Delta u_P^\mu + \int_{\tau_P}^{\tau} \Delta a^\mu(\tau') d\tau'. \quad (44)$$

Integrating once again finally results in

$$\Delta\gamma^\mu(\tau) = \Delta\gamma_P^\mu + \Delta u_P^\mu(\tau_D - \tau_P) + \int_{\tau_P}^\tau \int_{\tau_P}^{\tau'} \Delta a^\mu(\tau'') d\tau'' d\tau'. \quad (45)$$

By using our BC from equation (36) and (37), we are able to determine both constants of integration, i.e. $\Delta\gamma_P^\mu$ as well as Δu_P^μ :

$$0 \stackrel{!}{=} \Delta\gamma^\mu(\tau_P) = \Delta\gamma_P^\mu, \quad (46)$$

$$0 \stackrel{!}{=} \Delta\gamma^\mu(\tau_D) = \Delta u_P^\mu(\tau_D - \tau_P) + \int_{\tau_P}^{\tau_D} d\tau' \int_{\tau_P}^{\tau'} d\tau'' \Delta a^\mu(\tau''), \quad (47)$$

$$\Leftrightarrow \Delta u_P^\mu = -\Delta\bar{u}^\mu = \frac{-1}{\tau_D - \tau_P} \int_{\tau_P}^{\tau_D} d\tau' \int_{\tau_P}^{\tau'} d\tau'' \Delta a^\mu(\tau''). \quad (48)$$

Here we also defined $\Delta\bar{u}^\mu$, i.e. the average velocity correction between X_P and X_D . In total, the solution is given by

$$\gamma^\mu(\tau) = u^\mu(\tau - \tau_P) + X_P^\mu - \frac{\tau - \tau_P}{\tau_D - \tau_P} \int_{\tau_P}^{\tau_D} \int_{\tau_P}^{\tau'} \Delta a^\mu(\tau'') d\tau'' d\tau' + \int_{\tau_P}^\tau \int_{\tau_P}^{\tau'} \Delta a^\mu(\tau'') d\tau'' d\tau', \quad (49)$$

$$\Delta a^\mu(\tau) = -\frac{\eta^{\mu\nu}}{2} (2\partial_\alpha h_{\nu\beta} - \partial_\nu h_{\alpha\beta})|_{\gamma_0(\tau)} u^\alpha u^\beta. \quad (50)$$

Since this curve solves the geodesic equation to first order in epsilon and we have parametrized it with respect to the particles proper time, the on-shell condition

$$1 \equiv g_{\mu\nu}(\gamma(\tau)) \dot{\gamma}^\mu(\tau) \dot{\gamma}^\nu(\tau), \quad (51)$$

enforced by the BC, also holds along the whole trajectory. In our specific scenario the on-shell relation can be approximated as

$$1 \approx (\eta_{\mu\nu} + \epsilon h_{\mu\nu}(\gamma_0(\tau))) u^\mu u^\nu + \underbrace{2\eta_{\mu\nu} \Delta\epsilon \dot{\gamma}^\mu(\tau) u^\nu}_{(*)}. \quad (52)$$

The last term, (*), expands to

$$2\eta_{\mu\nu} \Delta\epsilon \dot{\gamma}^\mu(\tau) u^\nu = -\frac{2\epsilon}{\tau_D - \tau_P} \int_{\tau_P}^{\tau_D} \int_{\tau_P}^{\tau'} \eta_{\mu\nu} \Delta a^\mu(\tau') u^\nu d\tau' d\tau + 2\epsilon \int_{\tau_P}^\tau \eta_{\mu\nu} \Delta a^\mu(\tau') u^\nu d\tau', \quad (53)$$

where

$$2\eta_{\mu\nu} \Delta a^\mu(\tau') u^\nu = -2\eta_{\mu\nu} \frac{\eta^{\mu\sigma}}{2} (2\partial_\alpha h_{\sigma\beta} - \partial_\sigma h_{\alpha\beta})|_{\gamma_0(\tau)} u^\alpha u^\beta u^\nu \quad (54)$$

$$= -(2\partial_\alpha h_{\nu\beta} - \partial_\nu h_{\alpha\beta})|_{\gamma_0(\tau)} u^\alpha u^\beta u^\nu \quad (55)$$

$$= -\partial_\alpha h_{\nu\beta}(\gamma_0(\tau)) u^\alpha u^\beta u^\nu \quad (56)$$

$$= -\frac{d}{d\tau} (h_{\nu\beta}(\gamma_0(\tau)) u^\beta u^\nu). \quad (57)$$

Plugging this result back into (*) and using the fundamental theorem of calculus yields

$$2\eta_{\mu\nu} \epsilon \Delta\dot{\gamma}^\mu(\tau) u^\nu = \frac{\epsilon}{\tau_D - \tau_P} \int_{\tau_P}^{\tau_D} [h_{\alpha\beta}(\gamma_0(\tau)) u^\alpha u^\beta - h_{\alpha\beta}(X_P) u^\alpha u^\beta] d\tau \quad (58)$$

$$\begin{aligned} & -\epsilon [h_{\alpha\beta}(\gamma_0(\tau)) u^\alpha u^\beta - h_{\alpha\beta}(X_P) u^\alpha u^\beta] \\ & = \frac{\epsilon}{\tau_D - \tau_P} \int_{\tau_P}^{\tau_D} h_{\alpha\beta}(\gamma_0(\tau)) u^\alpha u^\beta d\tau - \epsilon h_{\alpha\beta}(\gamma_0(\tau)) u^\alpha u^\beta. \end{aligned} \quad (59)$$

Finally, substituting (*) back into the on-shell condition yields

$$1 \approx (\eta_{\mu\nu} + \epsilon h_{\mu\nu}(\gamma_0(\tau)))u^\mu u^\nu + \frac{\epsilon}{\tau_D - \tau_P} \int_{\tau_P}^{\tau_D} h_{\alpha\beta}(\gamma_0(\tau))u^\alpha u^\beta d\tau - \epsilon h_{\alpha\beta}(\gamma_0(\tau))u^\alpha u^\beta \quad (60)$$

$$= \eta_{\mu\nu}u^\mu u^\nu + \frac{\epsilon}{\tau_D - \tau_P} \int_{\tau_P}^{\tau_D} h_{\mu\nu}(\gamma_0(\tau))u^\mu u^\nu d\tau. \quad (61)$$

In the next section, we will use this result and the ultra relativistic approximation in order to obtain the correction to the spatial distance traveled by a neutrino in a GW spacetime.

B Modified Neutrino Path Length for general Gravitational Waves

Using equation (34) and the $\mathcal{O}(\epsilon)$ solution to the geodesic equation found in the last section, we are now able to compute the corrected physical length. First we show that $L(t_P, t_D) \approx t_D - t_P$ in the ultra relativistic limit and subsequently, we use this fact and the on-shell condition (61) to derive a relation between the physical, spatial distance between neutrino production and detection and the coordinate distance,

$$L_0 := \|\vec{X}_D - \vec{X}_P\|. \quad (62)$$

The latter distance may be identified with the flat spacetime distance, as the physical distance reduces to the coordinate distance for $h \equiv 0$. Indeed we will see that in most cases the physical distance oscillates around this flat spacetime value justifying that to some degree it still has physical significance.

First we prove that $L(t_P, t_D) \approx t_D - t_P$ by evaluating equation (34). Since we have already rewritten L in terms of $\dot{\gamma}^0$ using TT gauge this task is trivial:

$$L(t_P, t_D) = \int_{\tau_P=\tau(t_P)}^{\tau_D=\tau(t_D)} \left((\dot{\gamma}^0)^2 - 1 \right)^{\frac{1}{2}} d\tau \stackrel{\dot{\gamma}^0 \gg 1}{\approx} \int_{\tau_P}^{\tau_D} \dot{\gamma}^0 d\tau = t_D - t_P. \quad (63)$$

The other important ingredient is the deviation of the flow of proper time from the flat spacetime case quantified in equation (61),

$$1 = \eta_{\mu\nu}u^\mu u^\nu + \frac{\epsilon}{\tau_D - \tau_P} \int_{\tau_P}^{\tau_D} h_{\mu\nu}(\gamma_0(\tau))u^\mu u^\nu d\tau \quad (64)$$

$$\Leftrightarrow (u^0)^2 \approx \vec{u}^2 - \frac{\epsilon}{\tau_D - \tau_P} \int_{\tau_P}^{\tau_D} h_{\mu\nu}(\gamma_0(\tau))u^\mu u^\nu d\tau \quad (65)$$

$$\Leftrightarrow \frac{(t_D - t_P)^2}{(\tau_D - \tau_P)^2} \approx \frac{\|\vec{X}_D - \vec{X}_P\|^2}{(\tau_D - \tau_P)^2} - \frac{\epsilon}{\tau_D - \tau_P} \int_{\tau_P}^{\tau_D} h_{\mu\nu}(\gamma_0(\tau))u^\mu u^\nu d\tau \quad (66)$$

$$\Leftrightarrow t_D - t_P \approx \left[L_0^2 - \epsilon(\tau_D - \tau_P) \int_{\tau_P}^{\tau_D} h_{\mu\nu}(\gamma_0(\tau))u^\mu u^\nu d\tau \right]^{\frac{1}{2}} \quad (67)$$

$$\Leftrightarrow t_D - t_P \approx L_0 \left[1 - \epsilon(\tau_D - \tau_P) \frac{u^j u^k}{L_0 L_0} \int_{\tau_P}^{\tau_D} h_{jk}(\gamma_0(\tau)) d\tau \right]^{\frac{1}{2}} \quad (68)$$

$$\Leftrightarrow t_D - t_P \approx L_0 - \frac{\epsilon}{2} L_0 (\tau_D - \tau_P) \frac{u^j u^k}{L_0 L_0} \int_{\tau_P}^{\tau_D} h_{jk}(\gamma_0(\tau)) d\tau. \quad (69)$$

Here, we used that h is given in the TT gauge in order to eliminate all terms involving $h_{0\mu}$. Next, we exploit $L \approx t_D - t_P$ and $w^j = (X_D^j - X_P^j)/(\tau_D - \tau_P)$ and define the unit vectors $\hat{l}^j := (X_D^j - X_P^j)/L_0$ pointing into the direction of neutrino flow. Then we can write the physical length as

$$L(t_P, t_D) \approx L_0 - \frac{\epsilon}{2} \frac{L_0}{\tau_D - \tau_P} \hat{l}^j \hat{l}^k \int_{\tau_P}^{\tau_D} h_{jk}(\gamma_0(\tau)) d\tau. \quad (70)$$

Furthermore neglecting terms of $\mathcal{O}(\epsilon^2)$, we can write $\frac{L_0}{\tau_D - \tau_P} \approx u^0$. Thus the most general expression without further specifying $h_{\mu\nu}$ reads

$$L(t_P, t_D) \approx L_0 - \frac{\epsilon}{2} u^0 \int_{\tau_P}^{\tau_D} h_{\parallel}(\gamma_0(\tau)) d\tau, \quad (71)$$

$$h_{\parallel}(\gamma_0(\tau)) := \hat{l}^j \hat{l}^k h_{jk}(\gamma_0(\tau)). \quad (72)$$

We can make this formula more explicit by employing the Fourier decomposition of $h_{\mu\nu}$ in plane wave modes which is given by

$$h_{\mu\nu}(x) = \sum_{r \in \{+, \times\}} \int d^3 \vec{k} \operatorname{Re} \left[\Psi_r(\vec{k}) A_{\mu\nu}^r(\hat{k}) \exp(-ikx) \right], \quad (73)$$

where Ψ_r are the complex, scalar weight function (wave packets) of the corresponding modes and $A_{\mu\nu}^r(\hat{k})$ are the normalized polarization tensors depending only on the direction \hat{k} of the respective mode. Next we briefly discuss the polarization tensors and our choice of coordinates before we carry on the calculation of the integrated GW tensor along the neutrino trajectory.

A reasonable choice of coordinate system to describe the neutrino oscillation experiment of interest would be to define the coordinate axes such that the neutrino source resides at $\vec{X}_P \equiv 0$ and the detector remains at $\vec{X}_D \equiv L_0 \vec{e}_z$. This way we also assume that source and detector are not bound to each other by any forces since the physical length can vary freely as the GW passes through the system. Furthermore, we define the propagation direction of the GW with respect to this coordinate system. In order to obtain the parallel polarization components

$$A_{\parallel}^r(\hat{k}) := \hat{l}^j \hat{l}^k A_{jk}^r(\hat{k}), \quad (74)$$

which we need for our length expression, we simply rotate from the coordinate system, $\tilde{\Sigma}$, where $\hat{k} = \vec{e}_z$ to our system, Σ , using one rotation around the y axis with angle θ followed by a rotation around the z axis with angle φ . This yields

$$A_{\parallel}^r(\hat{k}) = \hat{l}^j \hat{l}^k A_{jk}^r(\hat{k}) \quad (75)$$

$$= R^m{}_j \hat{l}^j R^n{}_k \hat{l}^k \tilde{A}_{mn}^r(R^T \hat{k}) \quad (76)$$

$$= R^m{}_3 R^n{}_3 \tilde{A}_{mn}^r(\hat{e}_z) \quad (77)$$

$$= \begin{pmatrix} \cos(\varphi) \sin(\theta) \\ \sin(\varphi) \sin(\theta) \\ \cos(\theta) \end{pmatrix}^T \begin{pmatrix} A_{11}^r & A_{12}^r & 0 \\ A_{12}^r & -A_{11}^r & 0 \\ 0 & 0 & 0 \end{pmatrix} \begin{pmatrix} \cos(\varphi) \sin(\theta) \\ \sin(\varphi) \sin(\theta) \\ \cos(\theta) \end{pmatrix}, \quad (78)$$

where $A_{11}^+ = 1$, $A_{12}^+ = 0$ and $A_{11}^\times = 0$, $A_{12}^\times = 1$. Multiplying everything out, we get

$$A_{\parallel}^+(\hat{k}) = \sin^2(\theta)(\cos^2(\varphi) - \sin^2(\varphi)) = \sin^2(\theta) \cos(2\varphi), \quad (79)$$

$$A_{\parallel}^\times(\hat{k}) = 2 \sin^2(\theta) \cos(\varphi) \sin(\varphi) = \sin^2(\theta) \sin(2\varphi). \quad (80)$$

The angle θ describes the angle between the zeroth order neutrino trajectory and the GW propagation direction while φ quantifies the direction of the GW perpendicular to the neutrino trajectory.

Next, we decompose the complex wave functions Ψ_r into their absolute values and phases, i.e.

$$\Psi_r(\vec{k}) =: \psi_r(\vec{k}) \exp(-i\phi^r(\vec{k})), \quad (81)$$

leading us to the final expression for h_{\parallel} :

$$h_{\parallel}(x) = \sum_{r \in \{+, \times\}} \int d^3 \vec{k} \psi_r(\vec{k}) A_{\parallel}^r(\varphi, \theta) \cos(kx + \phi^r(\vec{k})). \quad (82)$$

Using this result, we can perform the integration along γ_0 explicitly and obtain a formula for ΔL in terms of the momentum distribution of h :

$$\Delta L(t_P, t_D) = -\frac{\epsilon}{2} u^0 \int_{\tau_P}^{\tau_D} h_{\parallel}(\gamma_0(\tau)) d\tau \quad (83)$$

$$= -\frac{\epsilon}{2} u^0 \sum_{r \in \{+, \times\}} \int d^3 \vec{k} \psi_r(\vec{k}) A_{\parallel}^r(\varphi, \theta) \int_{\tau_P}^{\tau_D} \cos(k\gamma^0 + \phi^r(\vec{k})) d\tau \quad (84)$$

$$= -\frac{\epsilon}{2} \sum_{r \in \{+, \times\}} \int d^3 \vec{k} \frac{u^0}{ku} \psi_r(\vec{k}) A_{\parallel}^r(\varphi, \theta) \int_{k\gamma_0(\tau_P) + \phi^r(\vec{k})}^{k\gamma_0(\tau_D) + \phi^r(\vec{k})} \cos(\xi) d\xi \quad (85)$$

$$\approx -\frac{\epsilon}{2} \sum_{r \in \{+, \times\}} \int d^3 \vec{k} \frac{\psi_r(\vec{k}) A_{\parallel}^r(\varphi, \theta)}{\omega(1 - \cos(\theta))} \int_{k\gamma_0(\tau_P) + \phi^r(\vec{k})}^{k\gamma_0(\tau_D) + \phi^r(\vec{k})} \cos(\xi) d\xi \quad (86)$$

$$= -\frac{\epsilon}{2} \sum_{r \in \{+, \times\}} \int d^3 \vec{k} \frac{\psi_r(\vec{k}) A_{\parallel}^r(\varphi, \theta)}{\omega(1 - \cos(\theta))} \left(\sin(kX_D + \phi^r(\vec{k})) - \sin(kX_P + \phi^r(\vec{k})) \right), \quad (87)$$

where $\omega = ||\vec{k}||$ and $\vec{u}\vec{k} \approx u^0 \omega \cos(\theta)$.

Again making use of our choice of coordinates, the ultrarelativistic limit and neglecting $\mathcal{O}(\epsilon^2)$ terms, we can write $X_P = (t, \vec{0})$ and $X_D = (t + L_0, L_0 \vec{e}_z)$ for some time t parameterizing the trajectories of neutrino source and detector. Thus, from now on we will also parametrize the distance deviation in terms of t , i.e.

$$\Delta L(t) \approx -\frac{\epsilon}{2} \sum_{r \in \{+, \times\}} \int d^3 \vec{k} \frac{\psi_r(\vec{k}) A_{\parallel}^r(\varphi, \theta)}{\omega(1 - \cos(\theta))} \left(\sin(\omega(t + L_0) - \omega L_0 \cos(\theta) + \phi^r(\vec{k})) - \sin(\omega t + \phi^r(\vec{k})) \right) \quad (88)$$

$$= -\frac{\epsilon}{2} \sum_{r \in \{+, \times\}} \int d^3 \vec{k} \frac{\psi_r(\vec{k}) A_{\parallel}^r(\varphi, \theta)}{\omega(1 - \cos(\theta))} \left(\sin \{ \omega(1 - \cos(\theta)) L_0 \} \cos(\omega t + \phi^r(\vec{k})) \right. \\ \left. + [\cos \{ \omega(1 - \cos(\theta)) L_0 \} - 1] \sin(\omega t + \phi^r(\vec{k})) \right). \quad (89)$$

Lastly, we want to consider the case of a sharply peaked momentum space wave packet, i.e.

$$\psi_r(\vec{k}) = a_r \delta_{\epsilon}^{(3)}(\vec{k} - \vec{K}), \quad (90)$$

where $\delta_{\epsilon}^{(3)}$ represents a sequence of functions converging to the delta distribution under the integral sign for $\epsilon \rightarrow 0$. In the case where all other functions than ψ_r are sufficiently weakly momentum dependent on the support of δ_{ϵ} we can pull them out of the integral and evaluate them at the peak momentum \vec{K} which yields

$$\Delta L(t) = -\frac{\epsilon}{2} \sum_{r \in \{+, \times\}} \frac{a_r A_{\parallel}^r(\varphi, \theta)}{\omega_K(1 - \cos(\theta))} \left(\sin \{ \omega_K(1 - \cos(\theta)) L_0 \} \cos(\omega_K t + \phi^r(\vec{K})) \right. \\ \left. + [\cos \{ \omega_K(1 - \cos(\theta)) L_0 \} - 1] \sin(\omega_K t + \phi^r(\vec{K})) \right). \quad (91)$$

C The influence of non-trivial Neutrino Trajectories on the Gravitational Wave Effect

Especially, when considering neutrinos in the solar system, the orientation of the GW and neutrino trajectories might vary non-trivially during the time of data taking. Usually this includes the motion of the neutrino detector and source relatively to each other and the orbit of their center of mass around the sun. Consequently this also has an non-negligible impact on the effect of the GW on the neutrino flavor transition probability since the angle between the GW direction \vec{k} and the zeroth order neutrino trajectory direction \vec{v} might become time

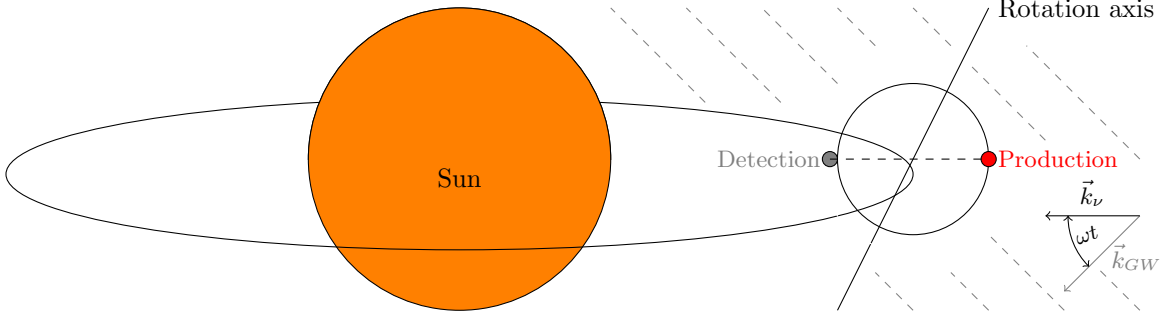


Figure 7: Illustration of the rotation of the detection and production region around the sun. The GW background is shown by the dashed gray lines with a resulting angle $\Theta(t)$ between the direction of propagation of the GW \vec{k}_{GW} and the neutrino propagation \vec{k}_ν .

dependent. Figure 7 illustrates the scenario just discussed. In the following, we assume that the relative motion of neutrino source and detector is negligible during the propagation time of a single neutrino. This will later allow us to repeat most of the steps of the derivation of ΔL shown in appendix B since during the integration over the neutrino path we can neglect the newly introduced time dependence. On the time scale of the neutrino oscillation experiment, however, the relative orientation of the neutrino velocity and GW vector as well as the GW tensor components may change significantly.

Assuming that the GW direction remains fixed in the sun's rest frame, $\tilde{\Sigma}$ described by coordinates \tilde{x}^μ , enables us to calculate the now time dependent GW parameters in the co-rotating center of mass system (CMS) of the neutrino source-detector system, Σ , via a coordinate change to the new coordinates x^μ (\tilde{x}^α). The corresponding GW tensors are, of course, related by the usual transformation law

$$h_{\alpha\beta}(x) = \frac{\partial \tilde{x}^\mu}{\partial x^\alpha} \frac{\partial \tilde{x}^\nu}{\partial x^\beta} \tilde{h}_{\mu\nu}(\tilde{x}(x)), \quad (92)$$

where the GW tensor in the sun's rest frame, $\tilde{h}_{\mu\nu}$, is still described by

$$\tilde{h}_{\mu\nu}(\tilde{x}) = \sum_{r \in \{+, \times\}} \int d^3 \vec{k} \psi_r(\vec{k}) A_{\mu\nu}^r(\hat{k}) \cos(k\tilde{x} + \phi^r(\vec{k})), \quad (93)$$

c.f. equation (73), where we take $\Psi_r = \psi_r \exp(-i\phi^r)$ with $\psi_r \geq 0$.

In order to find the GW tensor in the CMS of the neutrino experiment, our task now is to derive an expression for the coordinate transformation $\tilde{x}^\mu(x^\alpha)$. To that end, assume for simplicity that neutrino source and detector move at a constant coordinate distance L_0 , as described in appendix B. Now, let $X_P(t)$ and $X_D(t)$ be the trajectories of corresponding neutrino production and detection events, respectively. We define absolute and relative coordinates in $\tilde{\Sigma}$ by the relations

$$\left. \begin{aligned} \tilde{D}^\mu(t) &:= \frac{\tilde{X}_P^\mu(t) + \tilde{X}_D^\mu(t)}{2} \\ \tilde{r}^\mu(t) &:= \frac{\tilde{X}_D^\mu(t) - \tilde{X}_P^\mu(t)}{2} \end{aligned} \right\} \Leftrightarrow \left\{ \begin{aligned} \tilde{X}_P^\mu(t) &:= \tilde{D}^\mu(t) - \tilde{r}^\mu(t) \\ \tilde{X}_D^\mu(t) &:= \tilde{D}^\mu(t) + \tilde{r}^\mu(t) \end{aligned} \right. , \quad (94)$$

where $\|\vec{\tilde{r}}(t)\| \equiv L_0/2$ and $\tilde{r}^0(t) \equiv L_0/2$ at zeroth order in the GW and using the ultrarelativistic approximation. Thus, at most \tilde{r} performs a rotating motion in $\tilde{\Sigma}$. We specify the coordinate system Σ by demanding that

- $t = \tilde{t}$
- $\vec{D}(t) \equiv 0$
- $\vec{r}(t) \equiv \frac{L_0}{2} \vec{e}_z$

leading to the transformation law

$$\left. \begin{aligned} t(\tilde{x}) &= t \\ \vec{x}(\tilde{x}) &= R^T(\vec{\Phi})R^T(\vec{\Theta}(t)) \left(\vec{x} - \vec{D}(\tilde{t}) \right) \end{aligned} \right\} \Leftrightarrow \left\{ \begin{aligned} \tilde{t}(x) &= t \\ \vec{x}(x) &= \vec{D}(t) + R(\vec{\Theta}(t))R(\vec{\Phi})\vec{x} \end{aligned} \right. , \quad (95)$$

where $\Theta(t)$ is the axis (and angle) of rotation about which \vec{r} rotates in $\tilde{\Sigma}$ and $\vec{\Phi}$ is the rotation axis (and angle) needed to rotate $L_0 \cdot \hat{e}_z/2$ to $\vec{r}(0)$. From now on, we only refer to this combination of rotations as $O(t) := R(\vec{\Theta}(t))R(\vec{\Phi})$. The components of the Jacobian of this coordinate transformation thus read

$$\frac{\partial \tilde{x}^0}{\partial x^0} = 1, \quad \frac{\partial \tilde{x}^0}{\partial x^k} = 0, \quad \frac{\partial \tilde{x}^j}{\partial x^0} = \dot{D}^j(t) + \dot{O}^j_l(t)x^l, \quad \frac{\partial \tilde{x}^j}{\partial x^k} = O^j_k(t). \quad (96)$$

And the GW tensor becomes

$$\begin{aligned} h_{\alpha\beta}(\tilde{x}) &= (O^\mu_\alpha(t) + \delta^\mu(t)\delta_{\alpha 0}) (O^\nu_\beta(t) + \delta^\nu(t)\delta_{\beta 0}) \\ &\times \sum_{r \in \{+, \times\}} \int d^3\vec{k} \psi_r(\vec{k}) A_{\mu\nu}^r(\hat{k}) \cos\left(\omega t - \vec{k}^T O^T(t)(\vec{x} - \vec{D}(t)) + \phi^r(\vec{k})\right) \\ &= \sum_{r \in \{+, \times\}} \int d^3\vec{k} \psi_r(\vec{k}) O^\mu_\alpha(t) O^\nu_\beta(t) A_{\mu\nu}^r(\hat{k}) \cos\left(\omega t - (O(t)\vec{k})^T \vec{x} + (O(t)\vec{k})^T \vec{D}(t) + \phi^r(\vec{k})\right) \\ &+ \delta_{\alpha 0} \sum_{r \in \{+, \times\}} \int d^3\vec{k} \psi_r(\vec{k}) \delta^\mu(t) O^\nu_\beta(t) A_{\mu\nu}^r(\hat{k}) \cos\left(\omega t - (O(t)\vec{k})^T \vec{x} + (O(t)\vec{k})^T \vec{D}(t) + \phi^r(\vec{k})\right) \\ &+ \delta_{\beta 0} \sum_{r \in \{+, \times\}} \int d^3\vec{k} \psi_r(\vec{k}) O^\mu_\alpha(t) \delta^\nu(t) A_{\mu\nu}^r(\hat{k}) \cos\left(\omega t - (O(t)\vec{k})^T \vec{x} + (O(t)\vec{k})^T \vec{D}(t) + \phi^r(\vec{k})\right) \\ &+ \delta_{\alpha 0} \delta_{\beta 0} \sum_{r \in \{+, \times\}} \int d^3\vec{k} \psi_r(\vec{k}) \delta^\mu(t) \delta^\nu(t) A_{\mu\nu}^r(\hat{k}) \cos\left(\omega t - (O(t)\vec{k})^T \vec{x} + (O(t)\vec{k})^T \vec{D}(t) + \phi^r(\vec{k})\right), \end{aligned} \quad (97)$$

where we define $\delta^j = \dot{D}^j(t) + \dot{O}^j_l(t)x^l$ and $\delta^0 = 0$. To simplify this expression, we perform an orthogonal transformation of the integration variable $\vec{q} = O(t)\vec{k}$ which we then rename to \vec{k} again. Furthermore, we exploit the transformation behavior of the polarization tensor $A_{\mu\nu}(R\hat{k}) = R^\alpha_\mu R^\beta_\nu A_{\alpha\beta}(\hat{k})$ and define $\chi^r(\vec{k}, t) := \phi^r(\vec{k}) + \vec{k}^T \vec{D}(t)$. This yields

$$\begin{aligned} h_{\alpha\beta}(\tilde{x}) &= \sum_{r \in \{+, \times\}} \int d^3\vec{k} \psi_r(O^T \vec{k}) A_{\alpha\beta}^r(\hat{k}) \cos\left(\omega t - \vec{k} \cdot \vec{x} + \chi^r(\vec{k}, t)\right) \\ &+ \delta_{\alpha 0} \sum_{r \in \{+, \times\}} \int d^3\vec{k} \psi_r(\vec{k}) \delta^\mu(t) O^{T\rho}_\mu A_{\rho\beta}^r(\hat{k}) \cos\left(\omega t - \vec{k} \cdot \vec{x} + \chi^r(\vec{k}, t)\right) \\ &+ \delta_{\beta 0} \sum_{r \in \{+, \times\}} \int d^3\vec{k} \psi_r(\vec{k}) \delta^\nu(t) O^{T\sigma}_\nu A_{\alpha\sigma}^r(\hat{k}) \cos\left(\omega t - \vec{k} \cdot \vec{x} + \chi^r(\vec{k}, t)\right) \\ &+ \delta_{\alpha 0} \delta_{\beta 0} \sum_{r \in \{+, \times\}} \int d^3\vec{k} \psi_r(\vec{k}) \delta^\mu(t) O^{T\rho}_\mu \delta^\nu(t) O^{T\sigma}_\nu A_{\sigma\rho}^r(\hat{k}) \cos\left(\omega t - \vec{k} \cdot \vec{x} + \chi^r(\vec{k}, t)\right). \end{aligned} \quad (99)$$

One can immediately notice that this coordinate system does not belong to the TT gauge orbit since $h_{0\mu} \neq 0$ in general. Thus in the most general case we get corrections to ΔL from the non-inertial coordinate transformation we just discussed. However, when considering sufficiently slow motion of the coordinate system during the propagation of a single neutrino, i.e.

$$(t_D - t_P) \cdot |\dot{\delta}^j(t)| \ll 1, \quad (100)$$

we can actually neglect these terms in our expression in ΔL as being of higher than linear order in small quantities. Thus in this approximation the TT gauge condition holds again and we can proceed to calculate ΔL as before in appendix B, yielding

$$\Delta L(t) \approx -\frac{\epsilon}{2} \sum_{r \in \{+, \times\}} \int d^3 \vec{k} \frac{\psi_r(O^T(t) \vec{k}) A_{\parallel}^r(\hat{k})}{\omega - \vec{k} \vec{v}} \left(\sin(k X_D(t) + \chi^r(\vec{k}, t)) - \sin(k X_P(t) + \chi^r(\vec{k})) \right). \quad (101)$$

In order to obtain a better impression on what changes compared to the case discussed in appendix B, we now apply the inverse integral transform as before leading to

$$\Delta L(t) \approx -\frac{\epsilon}{2} \sum_{r \in \{+, \times\}} \int d^3 \vec{k} \frac{\psi_r(\vec{k}) A_{\parallel}^r(O(t) \hat{k})}{\omega - \vec{k} O(t) \vec{v}} \left(\sin(k O(t) X_D(t) + \chi^r(\vec{k}, t)) - \sin(k O(t) X_P(t) + \chi^r(\vec{k})) \right). \quad (102)$$

Therefore, we see that the relative orientation of the neutrino trajectory and the GW direction now changes with time, as expected, implying a variable influence of the effect. If for example \vec{k} becomes (anti-)parallel to \vec{v} the polarization vector vanishes and the corresponding mode doesn't contribute anymore.

D Toy Analysis: Likelihoods

In this section, we discuss the statistical procedure used to obtain the exclusion limits for the GW parameter space. First, we describe the setup of a toy experiment roughly modeling a typical neutrino oscillation experiment. Afterwards, we describe likelihood ratio tests and how we use them in order to obtain the allowed parameter space of our model for a given toy data set generated assuming no GW background.

D.1 Experimental Data Model

We attempt to model the unfolded experimental neutrino event counts for each flavor. To keep things simple since this is meant to be a proof of principle analysis rather than a complete experimental treatment, we neglect the following effects:

- Matter effects
- Systematic uncertainties like detector efficiency, accuracy and acceptance
- The procedure of unfolding the measured data
- Theoretical uncertainties

Furthermore, we do not simulate multiple data sets by sampling random event counts from the corresponding Poisson distribution. Instead, we take the underlying theory prediction for the expected number of events as the outcome of our experiment. The details of the statistical methods employed in this work will be described in the next subsection.

Regarding the experimental setup, we take into account the finite energy resolution and the binning of neutrino counts. Moreover, experiments never directly measure the flavor transition probabilities, but only in convolution with the energy flux spectrum. The form of this spectrum mostly depends on the origin of neutrinos, e.g. an energy power-law for atmospheric and astrophysical neutrinos.

Therefore, we need to compute the expected number of events from the combined probability distribution function (pdf):

$$\rho_b(E, L) = \sum_a \varphi_a(E) P_{ab}(E, L_0), \quad (103)$$

where φ_a is the normalized neutrino flux for an initial flavor a and P_{ab} is the transition probability of a neutrino from flavor a to flavor b . Since we aim to predict the event count for each energy bin, we need the accumulated

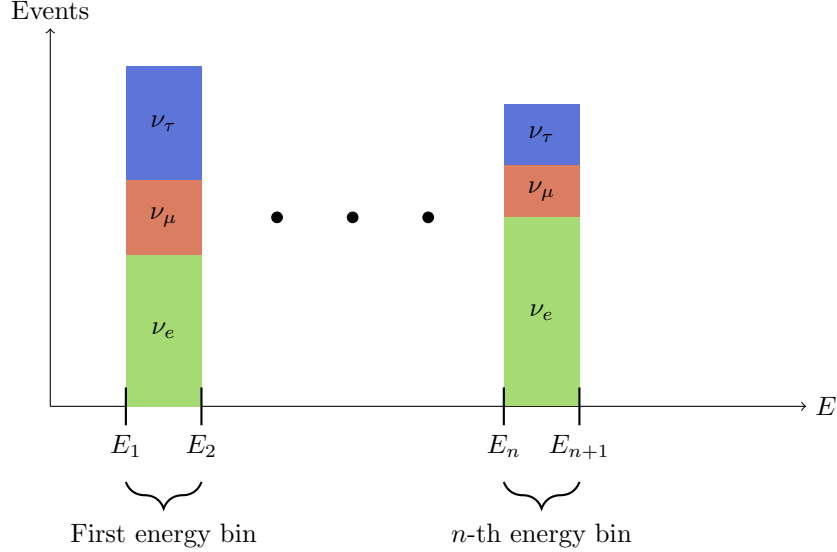


Figure 8: Illustration of the number of events for each flavor in the different energy bins.

probability for the respective energy ranges. Thus, for the i -th energy bin and flavor b we arrive at the final discrete probabilities:

$$p_{ib}(L_0) := \int_{E_i}^{E_{i+1}} \rho_b(E, L_0) dE, \quad (104)$$

where E_i and E_{i+1} are the lower and upper bin edges of the i -th bin as illustrated in figure 8.

Finally, we want to turn towards modeling the neutrino flux spectrum. We will especially discuss the neutrino flux expected from natural neutrino sources, i.e. atmospheric and astrophysical neutrinos, and that expected from fixed target experiments. As already mentioned, in the simplest scenario a naturally produced flux spectrum can be approximated by a power law energy dependence, i.e.

$$\varphi_a(E) = \frac{c_a}{\phi} E^{-\gamma}, \quad (105)$$

where $\gamma > 1$, c_a determines the flavor composition of the source flux and ϕ is a normalization constant such that

$$1 = \sum_a \int_{E_{\min}}^{E_{\max}} \varphi_a(E) dE. \quad (106)$$

Here, E_{\min} and E_{\max} are the minimum and maximum energies of neutrinos emerging from the source, respectively. Hence, in total we arrive at

$$\varphi_a(E) = (\gamma - 1) \frac{c_a}{\sum_b c_b} \frac{E^{-\gamma}}{\left(E_{\min}^{1-\gamma} - E_{\max}^{1-\gamma}\right)}. \quad (107)$$

A typical flavor composition of a neutrino source based on pion decay would for example be $\vec{c} = (c_a)_{a=1}^3 = (1, 2, 0)$.

For a fixed target experiment the precise shape of the flux depends on the details of the neutrino production mechanism. In order to keep our considerations simple, we do not specify a particular production process but approximate the neutrino energy spectrum by a Gaussian shape in order to account for the fact that artificially produced neutrino spectra usually peak at some mean energy \bar{E} and exhibit some width σ_E . We adopt this rather crude approximation, since our effect is not sensitive to the exact shape of the energy spectrum. It is

rather the location of the energy peak determining if an effect is visible. Therefore, in the currently considered setting the neutrino flux spectrum reads

$$\varphi_a(E) = \frac{c_a}{\phi} \exp\left(-\frac{1}{2} \left(\frac{E - \bar{E}_a}{\sigma_{E,a}^2}\right)^2\right), \quad (108)$$

where the normalization constant is given by

$$\phi = \sum_a c_a \sigma_{E,a} \sqrt{\frac{\pi}{2}} \left(\operatorname{erf}\left(\frac{E_{\max} - \bar{E}_a}{\sqrt{2}\sigma_{E,a}}\right) - \operatorname{erf}\left(\frac{E_{\min} - \bar{E}_a}{\sqrt{2}\sigma_{E,a}}\right) \right). \quad (109)$$

D.2 Likelihood Ratio Tests

In order to tell which parameter configurations (h, λ) or (h, f) , i.e. GW strain and wave length or frequency, lead to observable differences in comparison to the scenario where no GW is present, we use a likelihood ratio test. This method is especially suitable to tell differences between nested theoretical models, i.e. models belonging to the same class differing only in their respective parameter configurations. In our case, the *standard* scenario is represented by the parameter configuration $h = 0$.

In general the *test statistic* for this test is the *negative logarithmic likelihood ratio* (NLLR) given by

$$\Lambda(\vec{X}) = -2 \ln \left(\frac{\sup_{\vec{\vartheta} \in \Theta_0} \mathcal{L}(\vec{\vartheta} | \vec{X})}{\sup_{\vec{\vartheta} \in \Theta} \mathcal{L}(\vec{\vartheta} | \vec{X})} \right) \in [0, \infty), \quad (110)$$

where \vec{X} is a set of observations, $\vec{\vartheta}$ is the vector of parameters, Θ_0 is the space of parameter configurations corresponding to the *null hypothesis* (H_0) and Θ represents the space of all possible parameter configurations. If *Wilk's theorem* applies, Λ follows a χ^2 distribution with $d := \dim(\Theta) - \dim(\Theta_0)$ degrees of freedom (dof).

In our scenario, Θ_0 is a single point in our parameter space, i.e. $\vec{\vartheta}_0 = (h_0, \lambda_0)$, while Θ is the whole space of (h, λ) pairs. Moreover, all conditions of Wilk's theorem are fulfilled:

- $\Theta_0 \subset \Theta$: Since $\Theta_0 = \{\theta_0\}$ consists of a single point θ_0 in $\Theta = \mathbb{R} \times (0, \infty)$
- The optimum parameter configuration lies in the interior of Θ : $\theta_{\max} = (0, \lambda)$ where $\lambda \in (0, \infty)$ is arbitrary.

Thus, assuming sufficiently high event rates, Λ follows a χ^2 distribution with 2 dof. As we consider counting experiments, our likelihood function is given by a product of Poisson distributions, i.e.

$$\mathcal{L}(h, \lambda | \vec{n}) = \prod_{b=1}^{n_f} \prod_{i=1}^n \operatorname{Pois}(n_{ib}, \eta_{ib}(h, \lambda)), \quad (111)$$

where η_{ib} denotes the theoretical expected value of events in bin i and flavor b :

$$\eta_{ib}(h, \lambda) = p_{ib}(h, \lambda) N_{\text{tot}}. \quad (112)$$

Here N_{tot} is the total number of neutrino events.

Subsequently, the NLLR of our model reads

$$\Lambda(\vec{n}) = -2 \ln \left(\frac{\mathcal{L}(h_0, \lambda_0)}{\sup_{(h, \lambda) \in \mathbb{R}^2} \mathcal{L}(h, \lambda)} \right), \quad (113)$$

expanding to

$$\Lambda(\vec{n}) = -2 \sum_{i,b} [n_{ib} (\ln(\eta_{ib}(h_0, \lambda_0)) - \ln(\eta_{ib}(h^*, \lambda^*))) - (\eta_{ib}(h_0, \lambda_0) - \eta_{ib}(h^*, \lambda^*))], \quad (114)$$

Table 3: Values of the three chosen frequency ranges f_{GW} , wavelengths λ_{GW} , baselines L_0 , wave packet widths σ_x and estimated strain h sensitivity for keV neutrinos. For all benchmark points we assume $E \in [1, 10]$ keV with a bin width of $\Delta E \sim 0.45$ keV.

$f_{\text{GW}} / \text{Hz}$	$\lambda_{\text{GW}} / \text{km}$	L_0 / km	σ_x / m	h
1–10	10^7 – 10^8	$\sim 10^5$	4×10^{-3}	10^{-8}
10^{-6} – 10^{-5}	10^{10} – 10^{11}	$\sim 10^8$	4	10^{-11}
10^{-9}	10^{17}	$\sim 10^{10}$	4×10^2	10^{-13}

where h^* and λ^* are the parameters maximizing the likelihood on Θ .

For H_0 we assume that (h_0, λ_0) , i.e. a certain combination of GW parameters, are the underlying parameters of the given data set. We then proceed as follows: We generate a data set representing the expected number of neutrino events if no GW is present. Then a grid of parameter configurations (h_0, λ_0) is scanned and the corresponding NLLR values are compared to the α -quantile value Λ_α obtained from the χ^2 distribution with 2 dof. If $\Lambda(\vec{n}) > \Lambda_\alpha$ the null hypothesis is rejected meaning that the GW parameters would lead to an observable effect at $(1 - \alpha) \times 100\%$ confidence level.

E Neutrinos from within the Solar System with Large Wave Packet Widths

We observe that SM neutrinos with feasible wave packet widths can only provide weak constraints. To investigate the maximal limits achievable for SM neutrinos, we now consider the smallest still measurable energies possible in typical neutrino experiments, i.e. $E = \mathcal{O}(\text{keV})$. To estimate the lowest possible strain h in this scenario, we rearrange equation (16) and obtain:

$$h > \frac{8\pi r E}{L_0 \Delta m_{jk}^2}. \quad (115)$$

We are able to determine the wave packet width we need for achieving an observable effect with the right side of equation (16). Table 3 presents the values obtained in this process. The results of the analysis conducted with these parameters is depicted in figure 9. We find that significantly stronger constraints as low as $h \approx 10^{-13}$ with the longest baseline $L_{0,3}$ and the wavepacket width $\sigma_x = 4 \times 10^2$ m can be achieved in this manner. Interestingly this even results in an overlap with the sensitivity range of EPTA.

F Alternative Scenarios

In this appendix, we discuss the scenarios of adding new heavy neutrino flavours, meson mixing and an alternative experimental approach.

New Heavy Neutrino Flavor As we argued in the section 4.1 and 4.2, the sensitivity of neutrino oscillations to the GW strain h might improve for larger squared mass differences, Δm_{jk}^2 . Hence, in the following we want to turn our attention to exotic models involving heavy sterile neutrinos. For simplicity we consider the addition of a fourth neutrino generation mostly mixing with the electron neutrino. Apart from that, we consider here the same experimental scenarios already discussed in section 4.1. In spite of the freedom of choosing Δm_{41}^2 , we need to take into account mass dependent upper limits on the mixing matrix element $|U_{e4}|^2$ [91–150]. The most stringent constraints are collected in figure 10 plotted against the mass of the fourth mass eigenstate. It can be seen that the constraints on the mixing angle are less stringent for small masses $\mathcal{O}(\text{eV})$ and for very high masses of $\mathcal{O}(100 \text{ GeV})$. It, therefore, seems intriguing to consider these high masses, such as $\Delta m_{41}^2 = 100 \text{ GeV}^2$; however, assuming a wave packet width of $\sigma_x = 1 \text{ nm}$, the condition from equation (16) that the coherence length

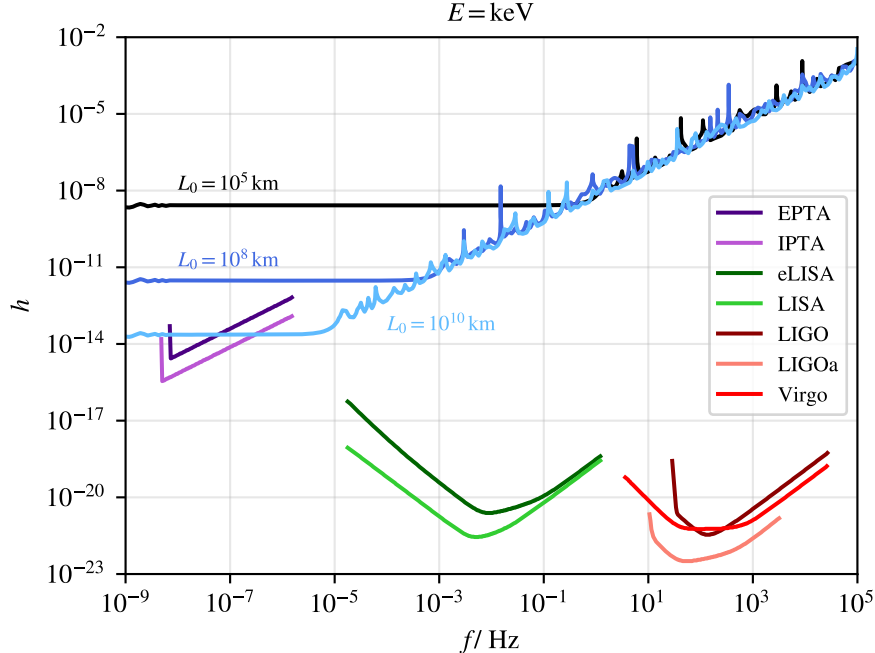


Figure 9: As figure 4, for wave packet widths from table 3.

L_{41}^{coh} must be larger than the considered baseline is only met for energies above the thresholds $E_{\text{thr},1} = 132 \text{ PeV}$, $E_{\text{thr},2} = 42 \text{ EeV}$ and $E_{\text{thr},3} = 420 \text{ EeV}$ for $L_{0,1}$, $L_{0,2}$ and $L_{0,3}$, respectively. These threshold energies are far beyond the energies achievable at colliders, so we do not consider them. At slightly smaller masses of a few keV to GeV, the mixing matrix element $|U_{e4}|^2$ is already strongly constrained. Therefore, the additional terms in the flavor transition probability describing the oscillation over the large mass gap would be suppressed by $|U_{e4}|^2 \lesssim 10^{-8}$. Consequently, the difference to the standard three neutrino case is nearly unobservable resulting in a very similar sensitivity to the GW strain h . In the light of these considerations, we concentrate on mass configurations of the order of 1–100 eV highlighted by the red crosses in figure 10.

In table 4 we show our choice of parameter configurations for the three interesting distances. There also the corresponding threshold energy E_{thr} , changing with the baseline L_0 and mass difference Δm_{41}^2 , is shown. The energy binning for each scenario is denoted by ΔE . We consider energy ranges around and slightly above the lowest energy allowed to ensure $L_{41}^{\text{coh}} > L_0$, c.f. criterion (ii) in section 3. Furthermore, condition (i) implies that by going to even higher energies the oscillation length increases implying weaker constraints on the GW strain, h , as can be seen in equation (115). For example, for a baseline of $L_{0,1} = 1000 \text{ km}$ and $\Delta m_{41}^2 = 1 \text{ eV}$ a minimum energy $E_{\text{thr}} = 0.01 \text{ GeV}$ is required which is why we consider energies between 10 MeV and 100 MeV. The parameters for the baseline $L_{0,2} = 10^8 \text{ km}$ and $L_{0,3} = 10^{10} \text{ km}$ follow the same reasoning. Due to the small, additional mixing angle θ_{14} we need to increase the number of events to $N = 10^9$ over 20 years in order to be able to resolve the high frequency oscillation over the sterile-active mass gap. Moreover, for the following analysis, we assume an initially pure electron neutrino fixed-target flux and that conditions (iv) and (v) are fulfilled by the neutrino source. Thus, the neutrino production region must fulfill $\Sigma_P \ll 25 \text{ m}$ for the lowest energies and $\Sigma_P \ll 442 \text{ km}$ for the highest energies under consideration.

Firstly, we consider atmospheric-like distances of $\mathcal{O}(1000 \text{ km})$, the results of the respective likelihood ratio test at 95% CL are depicted in figure 11. It can be observed that the contour line follows a similar shape to that of SM neutrinos we discuss in section 4.1 and with this configuration, we can achieve a minimal strain of $h \approx 10^{-4}$.

The 95 % CL NLLR contours in the f - h plane for baselines roughly of the order of the Mars–Earth distance are depicted in figure 12. Besides the typical behavior that the constraints for the strain h weaken with

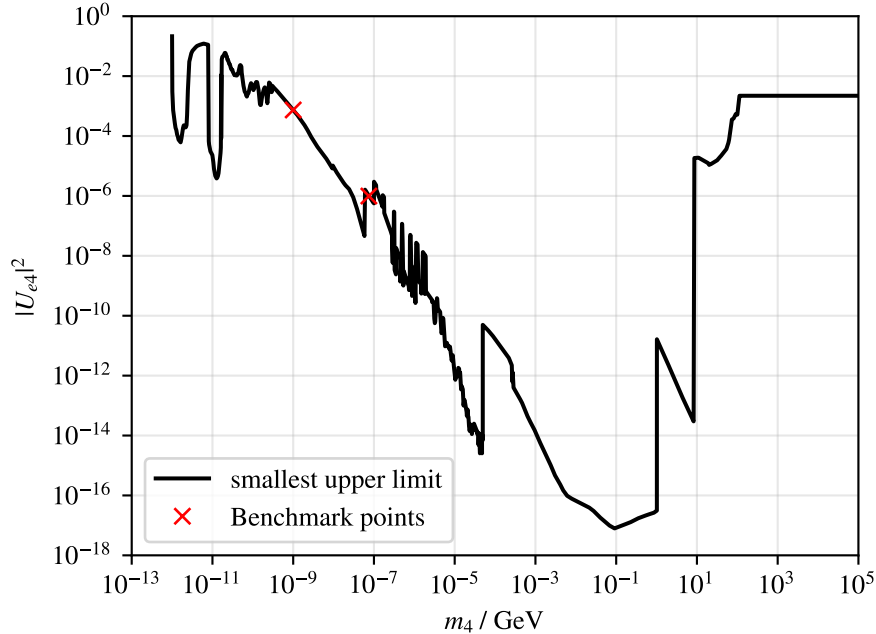


Figure 10: Shown are the bounds for the squared mixing matrix element $|U_{e4}|^2$ as a function of fourth mass eigenstate m_4 . The red crosses indicate the mass and mixing configurations chosen for the benchmark points in table 4 [91].

increasing neutrino energy, we also observe that the second TeV line, corresponding to the mass splitting $\Delta m_{41}^2 = 5.6 \times 10^3 \text{ eV}^2$, provides weaker constraints due to the smaller mixing angle compared to the $\Delta m_{41}^2 = 1 \text{ eV}^2$ scenario. Hence, the best constraints are achieved for a neutrino energy of GeV, where it is possible to probe strains of $h \approx 10^{-7}$.

Lastly, we also consider baselines corresponding to the radius of the solar system for heavy neutrinos. The results are shown in figure 13. Again, we observe the same, typical behavior of the contours, with the difference that this time the gap between the TeV contour lines is larger. This is due to the longer baseline, as the energy resolution needs to increase in order to probe the same oscillation lengths compared to smaller baselines. With a neutrino energy of GeV, neutrino experiments would be sensitive to strains of $h \approx 10^{-8}$.

Overall, it can be concluded that heavy neutrinos do not significantly improve the results for constraining GW parameters. The main reason for this is the small mixing matrix element $|U_{e4}|^2$ of at most $\mathcal{O}(10^{-3})$ for the scenarios of interest. Additionally, the choice of a realistic value for the width of the wave packets also plays a role in determining the effectiveness of constraining GW parameters. Both factors contribute to the overall sensitivity of the analysis and influence the ability to discern GW signatures in the presence of heavy neutrinos. Therefore, exotic scenarios involving hypothetical heavy, sterile neutrinos do not improve on the sensitivity for GWs compared with SM neutrinos.

Meson Mixing An alternative idea to use flavor oscillations as GW detectors may be to study meson oscillations instead. In particular oscillations of ultrarelativistic kaons seem intriguing in this regard as they provide large mass squared splittings and relatively long lifetimes. Since Kaon oscillations only occur as long as the beam is a coherent superposition of K_S and K_L the possible baselines are limited to (small) multiples of the mean decay length increasing with the Kaon energy. As the sensitivity to the GW strain grows with the baseline, very high energies are favorable. In the case of ultrarelativistic neutrinos the oscillation length also grows linearly with energy leading to a decrease of sensitivity equal to the increase gained from the larger baseline. We estimate that at best a sensitivity of $h \gtrsim 10^{-3}$ can be achieved. Thus, neutrino oscillations still seem to be

Table 4: Values of the three chosen GW frequency ranges f_{GW} , wavelengths λ_{GW} , baselines L_0 , various energies E , bin widths ΔE , mass splittings Δm_{41}^2 , mixing matrix elements $|U_{e4}|^2$ and threshold energies E_{thr} where effects would be observable for wave packet widths $\sigma_x = 1 \text{ nm}$.

$f_{\text{GW}} / \text{Hz}$	$\lambda_{\text{GW}} / \text{km}$	L_0 / km	E	ΔE	$\Delta m_{41}^2 / \text{eV}^2$	$ U_{e4} ^2$	$E_{\text{thr}} / \text{GeV}$
1–10	$10^4\text{--}10^5$	$\sim 10^3$	[10, 100]MeV	4.5 MeV	> 1	$< 7.4 \times 10^{-4}$	0.01
			[1, 10]GeV	0.45 GeV	> 1	$< 7.4 \times 10^{-4}$	4.20
$10^{-6}\text{--}10^{-5}$	$10^{10}\text{--}10^{11}$	$\sim 10^8$	[1, 10]GeV	0.45 GeV	> 1	$< 7.4 \times 10^{-4}$	4.20
			[1, 10]TeV	0.45 TeV	> 1	$< 7.4 \times 10^{-4}$	4.20
			[1, 10]TeV	0.45 TeV	$> 5.6 \times 10^3$	$< 10^{-6}$	314.63
10^{-9}	10^{17}	$\sim 10^{10}$	[10, 100]GeV	4.5 GeV	> 1	$< 7.4 \times 10^{-4}$	42.04
			[1, 10]TeV	0.45 TeV	> 1	$< 7.4 \times 10^{-4}$	42.04
			[1, 10]TeV	0.45 TeV	$> 5.6 \times 10^3$	$< 10^{-6}$	3146.34

the better choice for detecting GW signals via flavor oscillations even despite their small mass splittings.

Alternative Approach Another possible approach to measure the influence of GWs on neutrino oscillations would be to design an experiment detecting neutrinos precisely at energies on the verge of wave packet decoherence. Instead of introducing more decoherence into the system the influence of a GW could indeed also restore the coherence by shifting the baseline, accordingly. A possible experimental set-up could involve two phases of data taking where for example in the first phase decoherence is observed, while oscillations are restored in the second phase. In this case one could conclude that a GW of frequency $f \sim T_{\text{exp}}$ has passed through the neutrino trajectory. However, since this approach depends strongly on the phase of the GW only limited information can be expected.

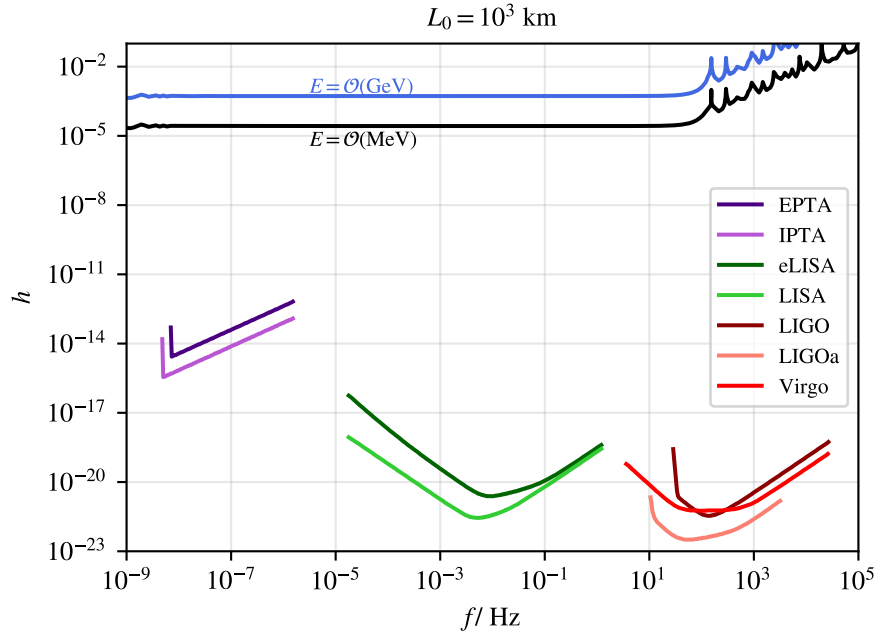


Figure 11: As figure 4, for the scenarios from the first major row of table 4.

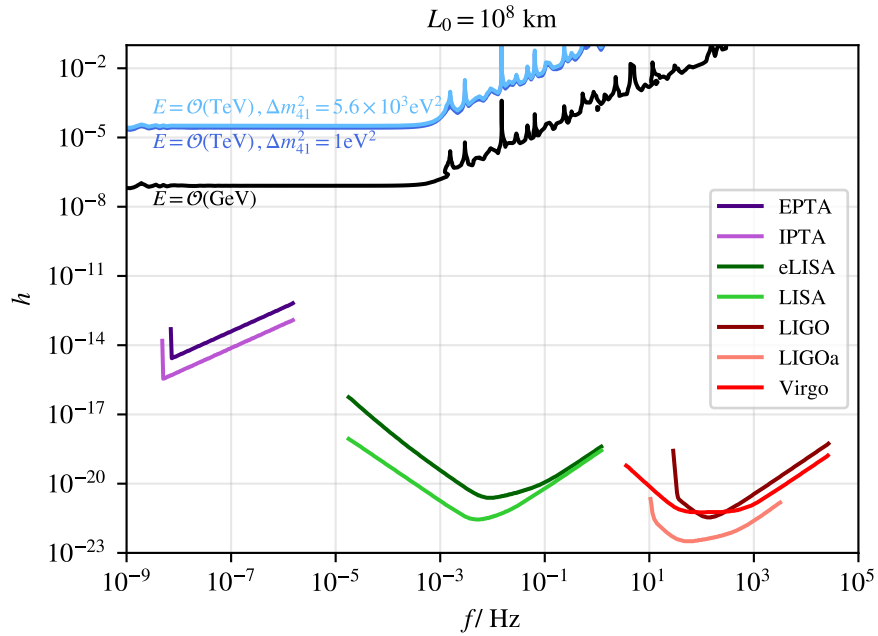


Figure 12: As figure 4, for the scenarios from the second major row of table 4.

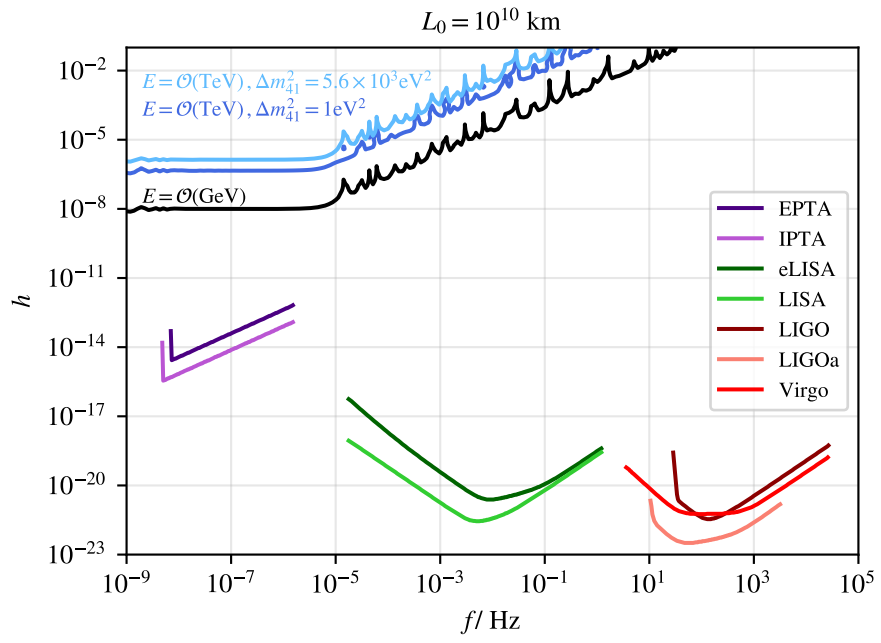


Figure 13: As figure 4, for the scenarios from the last major row of table 4.